LIMNOLOGY
and
OCEANOGRAPHY

ASLO

Limnol. Oceanogr. 9999, 2025, 1–20

doi: 10.1002/lno.70020

RESEARCH ARTICLE

Temporal methane dynamics in the surface waters of a stratified eutrophic lake over four years

César Ordóñez,[1*] **Alexandrine Massot**,[1] **Tonya DelSontro**,[1,a] **Timon Langenegger**,[1]
Daphne Donis,[1] **Daniel F. McGinnis**[1*]

Aquatic Physics Group, Department F.-A. Forel for Environmental and Aquatic Sciences (DEFSE), Faculty of Science, University of Geneva, Geneva, Switzerland

Abstract

The occurrence of oxic methane production (OMP) has been reported for numerous aquatic ecosystems. Its seasonal dynamics and contribution to global methane (CH_4) emissions remains uncertain, however, due to the lack of measurements constraining the spatial and temporal variability of OMP. In this study, we used data collected over 4 yrs with three types of models to estimate the net production/consumption of CH_4 (P_{net}) in the surface mixed layer of a eutrophic lake. These models allowed us to assess the lateral contribution and the surface fluxes' variability on P_{net} estimations. All model results show positive P_{net} rates suggesting that OMP occurs consistently during the stratified period and was often the dominant source of surface diffusive CH_4 emissions. In years with monthly data, we observed a consistent pattern of high P_{net} rates at the start of stratification and a decrease towards the end of the stratified season. Along with the P_{net} trends and in agreement with recent findings, correlations between P_{net} vs. Secchi depth, chlorophyll *a* concentrations and light climate suggest that photoautotrophs play a role in CH_4 production. Finally, using an isotopic mass balance model, we determined that the stable carbon isotopic signature of P_{net} in this lake was likely between −49‰ and −53‰, which aligns with published work. Clearly, OMP can be a significant component of an aquatic CH_4 budget of eutrophic systems, but can vary temporally; thus, temporal P_{net} variability should be considered when assessing the global contribution of OMP to aquatic CH_4 emissions, particularly in systems experiencing or threatened by eutrophication.

Over the last few decades, methane (CH_4) oversaturation in the surface oxic waters of oceans and lakes has been widely reported (termed "The Methane Paradox") (Lamontagne et al. 1973; Scranton and Brewer 1977; Tilbrook and Karl 1995; Karl et al. 2008; Tang et al. 2014). Although multiple mechanisms have been proposed for the presence of this CH_4, oxic methane production (OMP) has been proposed as one of the main explanations for the Methane Paradox (Lamontagne et al. 1973; Scranton and Brewer 1977; Grossart et al. 2011; Bogard et al. 2014; Donis et al. 2017; Günthel et al. 2019), contrasting with the understanding that CH_4 is only produced in anoxic environments (Conrad 2009). While several investigations have reported evidence that OMP occurs in the surface mixed layer (SML) of lakes (Grossart et al. 2011; Bogard et al. 2014; Donis et al. 2017; Günthel et al. 2019; Günthel et al. 2020), the seasonal patterns and main drivers of OMP remain unresolved.

About 20% of global warming can be attributed to CH_4, and freshwater systems are responsible for approximately 20–40% of the total CH_4 emissions to the atmosphere (49–202 $TgCH_4\ yr^{-1}$; Forster et al. 2021; Rosentreter et al. 2021; Saunois et al. 2024). Therefore, identifying the drivers of CH_4 sources and sinks in freshwater environments and their contributions to atmospheric CH_4 is crucial for understanding how the atmospheric CH_4 budget will evolve in a changing climate.

---

*Correspondence: cesar.ordonez@unige.ch; daniel.mcginnis@unige.ch

[a] Present address: Department of Earth and Environmental Sciences, University of Waterloo, Waterloo, Ontario, Canada

Associate editor: John Melack

Data Availability Statement: All relevant data included in this manuscript are available in https://doi.org/10.5281/zenodo.14911124.

Several mechanisms have been proposed for CH_4 production under oxic conditions in lakes (Wang et al. 2017; Khatun et al. 2019), the ocean (Karl et al. 2008; Repeta et al. 2016), and rivers (Alowaifeer et al. 2023). Recently, it was proposed that CH_4 is likely produced by any living organisms driven by the interplay of reactive-oxygen species, iron species, and methyl donors (Ernst et al. 2022). Interestingly, positive correlations between dissolved CH_4, oxygen and chlorophyll *a* (Chl *a*) concentrations suggest a role of phytoplankton in OMP (Bižić et al. 2020; Hartmann et al. 2020; Günthel et al. 2021). Moreover, the discovery that OMP follows light–dark cycles (Bižić et al. 2020; Hartmann et al. 2020) and is positively correlated with light and temperature (Klintzsch et al. 2020) indicates further links between OMP and photosynthesis. Since primary productivity varies seasonally as well as from lake to lake, it is likely that OMP dynamics also vary on the basis of trophic state, algal species, and/or light conditions.

An alternative explanation of the Methane Paradox is the transport of CH_4 from littoral sediments (Encinas Fernández et al. 2016; Peeters et al. 2019; Morana et al. 2020), although this mechanism alone has not been found fully to support the atmospheric diffusive CH_4 emissions from studied systems (Donis et al. 2017; Thottathil et al. 2022). In fact, recent studies show that OMP contribution to diffusive CH_4 emissions could fall between 0 % and 80 % in lakes during the stratified season using differential mass balance approaches (Donis et al. 2017; Günthel et al. 2019; Ordóñez et al. 2023). OMP occurs in surface waters (Tang et al. 2014; Donis et al. 2017) and, unlike anoxic environments such as anoxic sediments or the hypolimnion of stratified lakes, can be quickly emitted to the atmosphere. Several studies have focused on estimating the net production/consumption rate of CH_4 (P_{net}) in the SML, which is defined as the balance between OMP (that adds CH_4) and methane oxidation (MOx; that consumes CH_4). This means that when P_{net} is negative, MOx likely dominates over OMP, and when P_{net} is positive, OMP is likely higher than MOx. Despite the limited data on a temporal scale, Günthel et al. (2019), Ordóñez et al. (2023), and Liu et al. (2024) showed that P_{net} has a tendency to decrease towards the end of the summer. However, it is not known if this is driven by an increase in MOx rate, a decrease of the OMP rates or both.

Estimating OMP rates in aquatic systems has been approached using various methods. Incubation experiments in glass bottles have been used to directly measure OMP (Bižić et al. 2020; Günthel et al. 2020), but it is unclear how these controlled conditions might affect key variables driving OMP or MOx rates (such as light or oxygen) compared to natural lake environments. Other methods include using SML mass balance calculations (Donis et al. 2017; Günthel et al. 2019; Hartmann et al. 2020; Thottathil et al. 2022), lateral transport models (Encinas Fernández et al. 2016; Peeters et al. 2019; Ordóñez et al. 2023), and mesocosm studies (Bogard et al. 2014). While these methods can indirectly estimate P_{net} rates at the ecosystem-level from the CH_4 sources and sinks, incubation experiments are necessary to accurately determine OMP or MOx rates.

Given these complexities, we focused on studying P_{net}, as it represents the combination of all relevant biological processing of CH_4 in the surface layer (i.e., MOx and potential OMP) and directly contributes to diffusive CH_4 emissions to the atmosphere. To achieve this, we used measurements of various CH_4 components with a combination of mass balance calculations and modeling approaches to investigate the temporal dynamics of P_{net} during the stratified periods from 2016 to 2019 in Soppensee (Lake Soppen). While previous research in Soppensee has extensively examined hypolimnetic CH_4 dynamics (Vachon et al. 2019), oxidation rates (Langenegger et al. 2022), and ebullition (Langenegger et al. 2019), CH_4 dynamics in the SML of this lake have not been studied. Our comprehensive analysis includes results from this previous work to complete a full scale analysis of resulting CH_4 dynamics in the SML over multiple years. The use of multiple budgets and models allowed us to assess the temporal pattern of P_{net} and its contribution to diffusive CH_4 emissions. In addition, our measurements allowed us to evaluate the potential stable carbon isotopic signature of P_{net}, as well as account for alternative sources for surface CH_4 in Soppensee. Finally, we evaluated the upscaling approach proposed by Ordóñez et al. (2023) that estimates P_{net} rates using trophic parameters and found that approach also works in this eutrophic system, further highlighting the link between OMP and primary productivity.

Methods

Surface mass balance models

The full-scale mass balance (0-D) proposed by Donis et al. (2017), a wind-based mass balance (0-D) and the lateral transport model (1-D) proposed by Ordóñez et al. (2023) were used to estimate net production/consumption rates (P_{net}) in the SML of Soppensee during the stratified period from 2016 to 2019 (Fig. 1). P_{net} is considered the balance of OMP and MOx ($P_{\text{net}} = \text{OMP} - \text{MOx}$), which adds and removes CH_4 in the SML, respectively. Thus, when P_{net} is positive, the true OMP rate is higher than P_{net} because MOx is also simultaneously occurring. The full-scale mass balance model (Fig. 1c) estimates discrete P_{net} rates for each sampling campaign over the 4 yrs by considering measured sources and sinks of CH_4. In contrast, the wind-based mass balance model (Fig. 1d) continuously estimates P_{net} rates by using wind-driven k_{600} parameterization to calculate the flux to the atmosphere and by interpolating other sources and sinks of CH_4 over the same temporal resolution during the stratified periods of 2016, 2017, and 2018. Both models assume that the SML is well-mixed horizontally and vertically. The lateral transport model (Fig. 1e), however, does not assume horizontal mixing within the SML and instead estimates the lateral contribution of CH_4 due to transport from littoral sediments using CH_4 concentration transects from the shore to the center measured in 2018

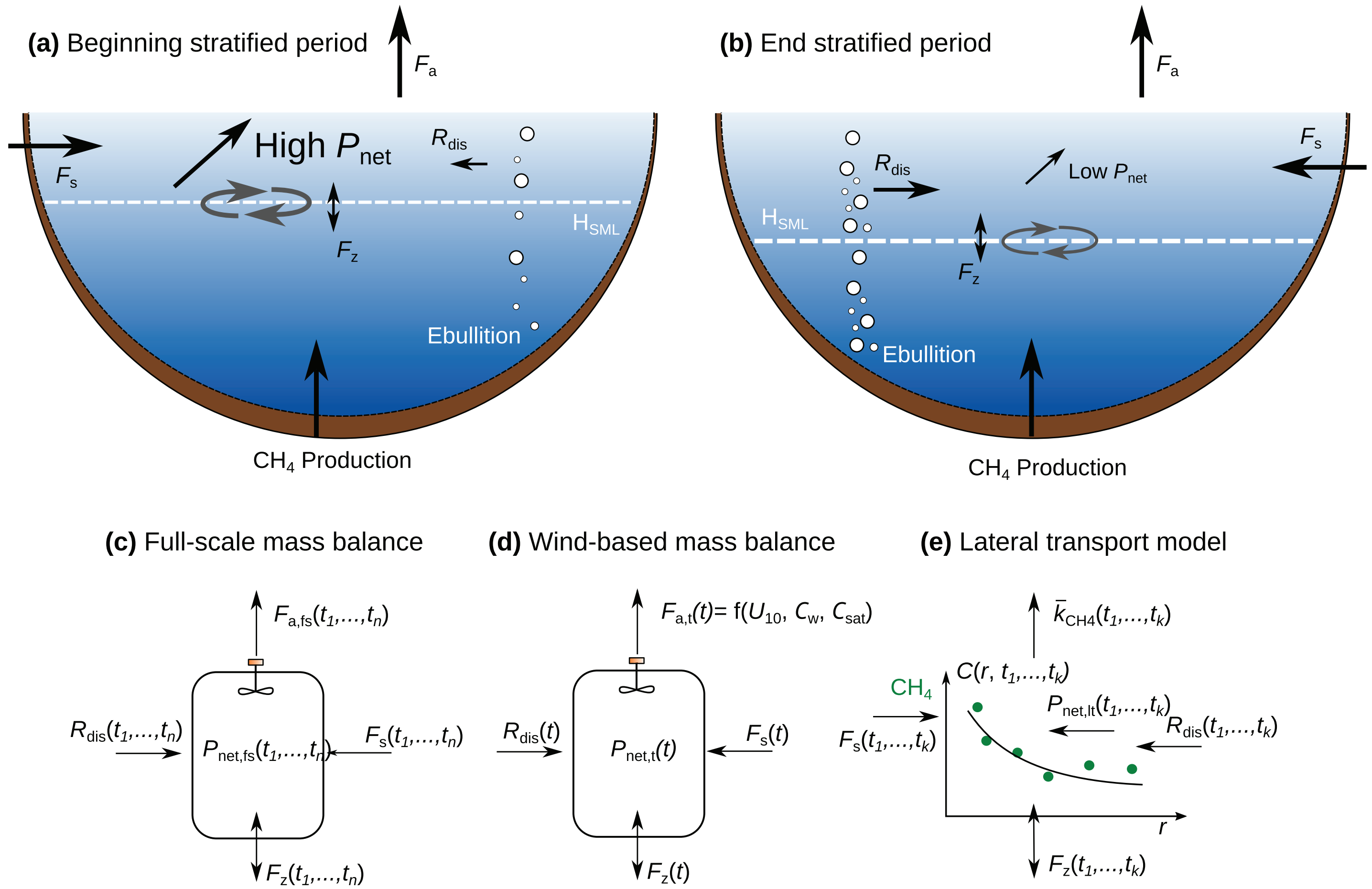

Fig. 1. Schematic representation of CH_4 fluxes in the surface mixed layer (SML) at the beginning (**a**) and at the end (**b**) of the stratified period, and methodological approaches. CH_4 is transported to the SML from littoral sediments (F_s), vertically via turbulent diffusion (F_z) and from the dissolution of bubbles (R_{dis}) originated from bottom sediments. The net CH_4 production/consumption (P_{net}) is considered as the balance of oxic CH_4 production (OMP) and CH_4 oxidation (MOx) and it is estimated using three models: (**c**) Full-scale mass balance, (**d**) wind-based model, and (**e**) lateral transport model. The full-scale and the wind-based mass balance models consider the SML as a well-mixed reactor while the lateral transport model uses horizontal dispersion to represent lateral transport. The full-scale mass balance and the lateral transport model use measured values to estimate discrete P_{net} rates at each sampling campaign ($t_1,\ldots,t_n$), with the lateral transport model being applied only when a transect of CH_4 concentrations was measured ($t_1,\ldots,t_k$). In contrast, the wind-based model estimates P_{net} rates continuously where each measured CH_4 component (except for diffusive emissions) was interpolated through time. In this model, diffusive CH_4 emission to the atmosphere (F_a) was estimated using literature mass transfer coefficient parameterizations as a function of wind speed (U_{10}), as well as dissolved CH_4 (C_w) and saturation (C_{sat}) concentrations. F_a was estimated using a chamber-based mass transfer coefficient ($\bar{k}_{CH_4}$) in the lateral transport model.

and 2019. Note that MOx rates are not essential for estimating P_{net}, they are, however, a prerequisite for calculating OMP. In this study, we determine P_{net} because it represents the component that directly influences diffusive emissions.

Full-scale mass balance

The net CH_4 production/consumption rate using the full-scale mass balance ($P_{net,fs}$) was determined in the SML during the stratified period (Eq. 1). This approach assumed that the SML can be modeled as a well-mixed reactor and the lateral contribution to the mass balance is equal to the littoral sediment flux times the littoral sediment area. The spatial average of the measured values of the CH_4 concentrations (C), the diffusive surface fluxes of CH_4 estimated from flux chambers ($F_{a,fs}$), the bubble dissolution in the SML (R_{dis}), the transport of CH_4 through the bottom of the SML (F_z), and the diffusive CH_4 flux from littoral sediments (F_s) were used as boundary conditions at each sampling campaign (Table 1).

$$\frac{\mathrm{d}C\forall_{\mathrm{SML}}}{\mathrm{dt}} = A_s(t)F_s - A_aF_{a,fs}(t) + A_z(t)F_z(t) + R_{dis}(t)\forall_{\mathrm{SML}}(t) + P_{net,fs}(t)\forall_{\mathrm{SML}}(t); \quad \left[\mathrm{mol\,d^{-1}}\right] \tag{1}$$

The SML volume ($\forall_{\mathrm{SML}}$), lake surface area (A_a), the littoral sediment area (A_s), and planar area at the bottom of the SML (A_z) are shown in Supporting Information Table S1. Both A_z and A_s were estimated based on the SML depth for every time step. Similar P_{net} rates were found under both steady-state and non-

Table 1. Measurements, model-derived parameters, and data sources analyzed from 2016 to 2019 over the stratified season.

Description	Symbol	Equation	Method	Period	Data source
Water column CH_4	C		Head space	Apr 2016 to Jan 2018	Vachon et al. (2019)
Water column CH_4	C		Head space	2018–2019	This study
Transect CH_4	C		Head space	May and Aug 2018 and Jul 2019	This study
Water column $\delta^{13}C_{CH_4}$	$\delta^{13}C_{CH_4}$		Head space	Apr 2016 to Jan 2018	Vachon et al. (2019)
Water column $\delta^{13}C_{CH_4}$	$\delta^{13}C_{CH_4}$		Head space	2018–2019	This study
Transect $\delta^{13}C_{CH_4}$	$\delta^{13}C_{CH_4}$		Head space	2018–2019	This study
Diff. CH_4 emissions	$F_{a,fs}$		Floating chambers	Apr 2016 to Jan 2018	Vachon et al. (2019)
Diff. CH_4 emissions	$F_{a,fs}$		Floating chambers	2018–2019	This study
Diff. CH_4 emission transect	$F_{a,fs}$		Floating chambers	May and Aug 2018 and Jul 2019	This study
Diff. CH_4 emissions	$F_{a,t}$	Eq. 2	k_{600} MacIntyre et al. (2010) parameterization	2016–2018	This study
Diff. CH_4 flux littoral sediments	$F_{s,pw}$	Eq. 6	Porewater from cut-syringe	2016–2019	Langenegger et al. (2022)
Diff. CH_4 flux littoral sediments	$F_{s,pw}$	Eq. 6	Porewater from Rhizons	2018–2019	This study
Diff. CH_4 flux littoral sediments	$F_{s,bc}$		Benthic chambers	2018–2019	This study
Total CH_4 eb. Flux below 8 m	F_{eb}		Inverted funnels	Apr 2016 to Jan 2018	Vachon et al. (2019)
CH_4 ebullition rate at SWI	R_{eb}		Bubble composition model	2018–2019	Langenegger et al. (2019) and this study
CH_4 flux at the bottom of SML	F_z	Eq. 9	Fick's first law	2016–2019	This study
CH_4 bubble dissolution rate in the SML	R_{dis}		McGinnis et al. (2006)	2016–2019	Langenegger et al. (2019); Vachon et al. (2019) and this study
Net CH_4 production or consumption rate	$P_{net,fs}$	Eq. 1	Full-scale mass balance	2016–2019	This study
Net CH_4 production or consumption rate	$P_{net,t}$	Eqs. 1 and 2	Wind-based mass balance	2016–2019	This study
Net CH_4 production or consumption rate	$P_{net,lt}$	Eq. 3	Lateral transport	2016–2019	This study

steady-state conditions (Supporting Information Fig. S1); therefore, only the steady-state condition is presented in the manuscript.

Wind-based mass balance

It is well known that the diffusive CH_4 emissions (F_a) varies in time and space depending on the turbulence level at the water surface due to wind velocity and convection (MacIntyre et al. 2010; MacIntyre et al. 2021), as well as the CH_4 concentration gradient across the air-water interface. To account for the natural temporal variability of F_a, we employed a wind-based mass balance model using continuously observed wind data to compute a temporally resolved F_a. We then linearly interpolated the other CH_4 components of the wind-based mass balance to obtain daily P_{net} rates during the stratified period ($P_{net,t}$, Eqs. 1 and 2). To calculate F_a, the following was used:

$$F_{a,t} = k_{CH_4}\left(C - H_{cp}P_{CH_4}\right); \quad \left[\mathrm{mmol\,m^{-2}\,d^{-1}}\right] \qquad (2)$$

The Henry constant of CH_4 dissolution at in situ temperature (H_{cp}) was obtained following Sander (2015). The atmospheric partial pressure of CH_4 (P_{CH_4}) was obtained from air samples taken at Soppensee and the local atmospheric pressure during each sampling campaign. The mass transfer coefficient for CH_4 (k_{CH_4}) was calculated following McGinnis et al. (2015), where the Schmidt number for CH_4 was estimated from the surface water temperature (Wanninkhof 1992), the exponent $n = 2/3$ when the wind speed at 10 m height (U_{10}) < $3.7\ \mathrm{m\,s^{-1}}$ or $n = 1/2$ when $U_{10} > 3.7\ \mathrm{m\,s^{-1}}$, and the standardized gas transfer coefficient (k_{600}) following MacIntyre et al. (2010) for negative buoyancy. This parameterization of k_{600} showed the best agreement between five tested parameterizations and the chamber-based k_{600} estimation

(Supporting Information Table S2). k_{600} for the wind-based mass balance model was estimated using daily average wind speed measured from a meteorological station situated about 12 km north of the lake (Egolzwil Station, Federal Office of Meteorology and Climatology MeteoSwiss). A portable weather station (Kestrel 5500) was sporadically deployed at the center of the lake during most campaigns. When we compared these lake level wind speed measurements and adjusted them to a 10 m height according to Crusius and Wanninkhof (2003), we computed lower U_{10} values compared to those measured at 10 m height at the Egolzwil station. This discrepancy can be attributed to the wind shelter effect created by the surrounding trees and hills around Soppensee, whereas the Egolzwil station is located in an open field. To account for this difference, we applied an empirical correction to estimate the U_{10} measured at Egolzwil under lake conditions ($U_{10,\mathrm{lake}} = 0.7 U_{10,\mathrm{Egolzwil}}$; Supporting Information Fig. S2).

Lateral transport model

The lateral transport model simulates transect CH_4 concentrations in the SML following Peeters et al. (2019) and modified according to Ordóñez et al. (2023) (Eq. 3). This model considers that the surface layer is fully mixed in the vertical, thereby resulting in uniform CH_4 concentrations with depth in the SML.

$$\begin{aligned}\frac{\partial C}{\partial t} = {} & K_{\mathrm{H}} \frac{1}{H(t,r) r} \frac{\partial}{\partial r}\left(H(t,r) r \frac{\partial C(t,r)}{\partial r}\right) \\ & + \frac{1}{H(t,r)} K_{\mathrm{z}}(t) \frac{C_{\mathrm{hyp}}(t) - C(t,r)}{\Delta z} \\ & - \frac{\bar{k}_{\mathrm{CH_4}}(t)}{H(t,r)} \left(C(t,r) - \mathrm{H_{cp}}(t) P_{\mathrm{CH_4}}(t)\right) \\ & + \frac{F_s(r)}{H(t,r)} + R_{\mathrm{dis}}(t,r) + P_{\mathrm{net,lt}}(t); \left[\mathrm{mol\,m^{-3}\,d^{-1}}\right]\end{aligned} \tag{3}$$

The mass transfer coefficient for CH_4 was calculated based on the average gas transfer coefficient obtained from the flux chambers ($\bar{k}_{\mathrm{CH_4}}$), as they have shown good agreement with the eddy covariance technique (Schubert et al. 2012) and have proven applicable in both lotic and lentic systems (Lorke et al. 2015). C_{hyp} is the CH_4 concentration 1 m below the bottom of the SML and $\Delta z = 1$ m. The model assumed that the SML, along with its sources and sinks, is radially symmetric in the horizontal plane. Consequently, the development of CH_4 concentration along the transect can be described based on the radial distance r from center to the shore of the lake ($r_{\max} = \sqrt{A_{\mathrm{a}}/\pi}$). The SML thickness ($H(r)$) is equal to the mixed layer depth in the pelagic zone ($r < r_{\mathrm{s}} = \sqrt{(A_{\mathrm{a}} - A_{\mathrm{s}})/\pi}$) and decreases linearly to zero at the shore. The sediment flux was considered equal to F_{s} and zero at the littoral and pelagic zone as:

$$F_s(r) = \begin{cases} \overline{F_{\mathrm{s}}} & \text{for } r \geq r_{\mathrm{s}} \\ 0 & \text{for } r < r_{\mathrm{s}} \end{cases} \quad \left[\mathrm{mmol\,m^{-2}\,d^{-1}}\right] \tag{4}$$

To estimate the horizontal dispersion coefficient (K_{H}) we used Peeters and Hofmann (2015) parameterization:

$$K_{\mathrm{H}} = 1.4 \times 10^{-4} L^{1.07}; \quad \left[\mathrm{m^2\,s^{-1}}\right] \tag{5}$$

where the length scale L (m) was calculated as $L = r = \sqrt{A_{\mathrm{a}}/\pi}$. Equation 5 is the average of the results 1, 3, and 4 found in table 2 of Peeters and Hofmann (2015).

$P_{\mathrm{net,lt}}$ rates for each date were calculated by minimizing the root-mean-square error between the simulated transect CH_4 concentrations to the measured CH_4 concentrations using an optimization solver implemented with the *curve fit* function from (Virtanen et al. 2020) in Python (Ordóñez 2023). Note that the lateral transport model was only applicable to May, July, and September 2018, and August 2019 campaigns when CH_4 concentration transects were systematically conducted.

Study site and sampling

The study was conducted in a small eutrophic lake, Soppensee (47.09°N, 8.08°E, 596 m above the sea level), located in Canton Lucerne, Switzerland. This glacially formed lake has a surface area of 0.24 km^2 and a maximal depth of 26 m. The lake watershed is about 1.6 km^2 and lies in an area of intense agriculture (Lotter 1989).

This study relies on data from the water column profiles of CH_4, the stable carbon isotopes of CH_4 ($\delta^{13}C_{\mathrm{CH_4}}$), temperature, dissolved oxygen (O_2), as well as CH_4 diffusive fluxes to the atmosphere and CH_4 ebullition rates during April 2016 to January 2018 from Vachon et al. (2019). Additional water column data were collected during 2018 and 2019 including surface CH_4 concentrations, $\delta^{13}C_{\mathrm{CH_4}}$ and surface diffusive fluxes to the atmosphere (F_{a}) along transects performed in May, July, and September 2018 and August 2019. Ten locations were sampled in each transect from the shore to the deepest point of the lake. The sample locations and the bathymetric map are shown in Supporting Information Fig. S3.

In the deepest point of the lake (M1; Supporting Information Fig. S3) temperature loggers (Vemco Minilog-II-T; ± 0.1 °C, resolution 0.01 °C) were moored from April 2016 to October 2019. Water temperature was measured every minute at several depths (Supporting Information Fig. S4). A dissolved O_2 probe (miniDot, Precision Measurements Engineering) was installed at ~ 1 m depth where temperature, dissolved O_2 concentration ($\mathrm{mgO_2\,L^{-1}}$), and saturation (%) were measured every minute from April 2016 to October 2019. In addition, manual CTD (Conductivity–temperature–depth) profiles were performed at M1 using a multiparameter sonde (EXO2 Yellow Spring Instrument, after May 2017 a Seabird SBE19plus CTD profiler). The EXO2 profiler was equipped with a temperature, conductivity, oxygen and pH sensor while the SBE19plus was equipped with the same parameters plus turbidity, photosynthetic active radiation, and Chl *a* sensors. The high resolution temperature (T) profiles were used to define the bottom of the SML as the depth from the surface where the temperature gradient transition from lower to higher than $-1\,^{\circ}\mathrm{C\,m^{-1}}$ (i.e., transitioning into the metalimnion) (Fee et al. 1996). Although several approaches exist to estimate the SML depth (Imberger 1985; Bernhardt and Kirillin 2013; Diaz et al. 2021), a visual assessment of the estimated SML depths as per this chosen approach suggests it effectively distinguishes the homogeneous temperature portion of the water column (i.e., the SML) from the region where temperature gradient increases (i.e., the metalimnion) (Supporting Information Figs. S4, S5). The stratified period was defined when the density difference between the surface and bottom water exceeded $0.7\,\mathrm{kg\,m^{-3}}$. Water density was calculated using T and the specific conductivity at 20°C (κ_{20}) from the CTD profiles (Imboden and Wüest 1995). In August 2016, May and September 2018, and August 2019, manual water profiles were performed with a spectrofluorometer (bbe Moldaenke GmbH) at the deepest point of the lake to measure total Chl *a* concentrations. Lower concentrations were found from measurements performed with the SBE19plus CTD profiler compared with the spectrofluorometer at the same time in the lake. Therefore, the average Chl *a* concentration was calculated as the average value in the SML measured with the spectrofluorometer and the corrected values from SBE19plus CTD profiler using an empirical correction (Supporting Information Fig. S6).

Diffusive CH_4 fluxes from littoral sediment (*see* definition below) from Langenegger et al. (2022) were included in our analysis. Additional littoral sediment cores were retrieved at the same locations (a, b, and c) reported by Langenegger et al. (2022) to determine CH_4 diffusive fluxes using benthic chambers and Rhizons (*see* Methods below). Finally, the Secchi disk depth was also measured at each sampling campaign after August 2016. An overview of the data used along with the associated time periods and sources is given in Table 1.

Water column CH_4 concentration and $\delta^{13}C_{CH_4}$ signature

The surface CH_4 concentrations and $\delta^{13}C_{CH_4}$ were measured using the methodology described by Vachon et al. (2019) for the water profiles and by Ordóñez et al. (2023) for the transect conducted during May, July, and September 2018 and August 2019. The transect measurements were considered as representative of daily average conditions (Table 1). For each sample, CH_4 concentration and its $\delta^{13}C_{CH_4}$ were measured using the headspace method following Donis et al. (2017). The samples were measured on a Cavity Ring-Down Spectrometer analyzer (Picarro G220-i) for CH_4 concentrations in the gas phase (ppm) and stable carbon isotopic ratios ($\delta^{13}C_{CH_4}$ in ‰). Water CH_4 concentrations were back calculated according to Wiesenburg and Guinasso (1979) accounting for water temperature, air concentration and the headspace/water ratio in the bottle. Water column profiles of CH_4 concentrations were measured at the deepest point of the lake (M1) and in May and September 2018 they were also measured at a 12-m deep point (M2) and along 10 surface water points in each transect. Since multiple depths were measured in the SML at M1 and M2 compared with only one value at the surface of each point in the transects, the average CH_4 concentration value in the SML at M1 and M2 was assumed as part of the transect to calculate the surface average CH_4 concentration for the entire lake. This procedure minimizes the bias that can be caused by the several measurements taken at M1 and M2 in comparison with only one sample for the rest of the transect. When transect data were not available, the average value for the entire lake was calculated with the CH_4 concentrations measured in the SML.

CH_4 diffusive fluxes to the atmosphere

The diffusive fluxes to the atmosphere (F_a) were estimated using a floating chamber attached to a portable GHG analyzer (UGGA; Los Gatos Research). The floating chamber consists of an inverted plastic container with foam elements for flotation (as McGinnis et al. 2015). Fluxes were obtained by the slopes of the resolved CH_4 curves over ~5 min when the slopes were approximately linear ($R^2 > 0.97$). F_a was measured at M1, and in May and September 2018, it was also measured at M2 and along the same transects where CH_4 concentrations were recorded (Table 1). Since multiple measurements were taken at M1 and M2, compared to a single measurement at each point along the transects, the average values from M1 and M2 were assumed as part of the transect to calculate the average flux F_a for the entire lake. Similar to the CH_4 concentrations, this approach minimizes the bias due to number of samples.

Sediment core extraction

Littoral sediment cores were retrieved at the same locations as the ones presented by Langenegger et al. (2022) (Cores a, b, and c; Supporting Information Table S1), where porewater concentrations were measured with Rhizons (Rhizosphere Research Products). The sediment cores were retrieved with a gravity sediment corer (Uwitech) equipped with an acrylic liner of 70 cm in length and with an internal diameter of 6 cm. The liner had pre-drilled holes every 1 cm to fit Rhizons and 1- and 3-mL syringes. Additional sediment cores were retrieved in those same locations and benthic chambers were used to calculate the CH_4 diffusive flux from the sediment cores. The location and depth of each core are shown in Supporting Information Fig. S3 and Table 2, respectively, and Rhizons and benthic chamber approaches are described below.

Porewater CH_4 concentration and $\delta^{13}C_{CH_4}$ signature

The Rhizons are porewater samplers designed to extract small volumes of water from soil and sediments in a minimally disturbing way. They are made of an inert microporous

Table 2. CH_4 diffusive flux from littoral sediments. Data from this work and previously published data from Langenegger et al. (2022) and Langenegger et al. (2019).

Core	Date	Water depth (m)	Temp (°C)	Diffusive flux ($mmol\ m^{-2}\ d^{-1}$) Benthic chamber	Rhizons	Cut-syringe	Average
C1	August 12, 2019	0.80	22.40	3.23	0.29	1.27	1.60
C2	August 12, 2019	1.00	22.40	2.38	0.05	3.14	1.86
C3	August 12, 2019	1.00	22.40	0.50	0.32	1.11	0.64
C4	July 10, 2017	3.00	23.70	-	-	1.43	1.43
C5	September 13, 2016	4.00	21.00	-	-	3.64	3.64
C6	July 10, 2017	6.00	10.30	-	-	0.22	0.22
Average sediment flux ($mmol\ m^{-2}\ d^{-1}$)							1.56 ± 1.19

tube (0.15 μm) that is connected to a needle through a flexible 1-mm tube. About 2 mL of porewater was extracted using the Rhizons and transported through a needle into evacuated and septum-capped 49 mL glass vials (Infocroma). Vials were filled with zero air to create a headspace and shaken vigorously for 2 min to allow the porewater and headspace to reach equilibrium. The headspace was extracted with a glass syringe (Fortuna Optima) by gently injecting zero air (Synthetic air 5.6, Pangas AG) into the vial with a second glass syringe prior to flushing the headspace three times between the two syringes.

Due to the fact that Rhizon measurements can be influenced by surrounding sediment, CH_4 concentrations in the porewater were also estimated using the cut-syringe method (Donis et al. 2017; Langenegger et al. 2019). Briefly, about 3 mL of sediment was subsampled with headless 3-mL syringes through pre-drilled holes in the core liner. The sample was immediately placed into 1-L glass bottle (Duran GmbH) containing 600 mL of lake water previously equilibrated with atmospheric air with an air stone. Subsequently, the same procedure as the water column headspace method was used.

The headspace for both methods was then measured with the Cavity Ring-Down Spectrometer analyzer (Picarro G220-i) directly from the glass syringe for CH_4 and $\delta^{13}C_{CH_4}$ concentrations in the gas phase. Methane concentrations were back-calculated using Wiesenburg and Guinasso (1979) accounting for water temperature, the headspace/water ratio in the vial, dilution effects from syringe extraction and sediment porewater (assuming equilibrium with the atmosphere), and a porosity of 0.9.

Methane diffusive fluxes from littoral sediments

The littoral CH_4 sediment flux (F_s) was determined using the porewater concentration profiles sampled with the Rhizon and cut-syringe methods as well as directly measured with benthic chambers (*see* below). To calculate sediment flux via the porewater profiles, we used Fick's First Law over the linear top 2–3 cm following:

$$F_{s,pw} = -\phi D_{CH_4} \theta^{-2} \frac{\partial C}{\partial z}; \quad \left[\mathrm{mmol\ m^{-2}\ d^{-1}} \right] \tag{6}$$

where $F_{s,pw}$ is the diffusive CH_4 flux at the sediment–water interface (SWI), ϕ is the porosity of the sediments (assumed to be 0.9), D_{CH_4} is the diffusion coefficient for CH_4 in water ($1.5\ m^2\ s^{-1}$; Broecker and Peng (1974)), θ^2 is the square of tortuosity (1.2; Boudreau (1997)), and $\partial C / \partial z$ is the measured vertical CH_4 concentration gradient at SWI.

Benthic chamber fluxes were measured directly in the littoral sediment cores immediately after retrieval ($F_{s,cb}$). A core lid was placed on the retrieved core leaving ~5 cm of headspace and ~30 – 50 cm of water. The lid was connected to a GHG analyzer (UGGA, Los Gatos Research) creating a closed loop where the partial pressure of CH_4 (P_{CH_4}) was measured over time. Each deployment lasted about 1 h while the surface water was stirred to increase the mass transfer coefficient at the air-water interface without producing resuspension. Dissolved CH_4 concentrations (C_w) in the overlying core water were measured at the beginning and at the end of the experiment. The fluxes were calculated based on the temporal change of CH_4 concentration inside the chamber as proposed by Ordóñez et al. (2023).

The final littoral sediment flux (F_s) was calculated as the average flux at each location (Table 1), determined as the average of all the methods (if several methods were applied in the same sediment core). The littoral sediment flux was assumed constant during the entire period of analysis.

Bubble CH_4 dissolution and ebullition rates

Ebullition rates at the SWI (R_{eb}) for the entire lake sediment in May, July, and September 2018, as well as August 2019, were determined using bubble composition measurements from those dates and diffusive sediment fluxes from measurements taken between 2016 and 2019 following Langenegger et al. (2019) (Table 1). Briefly, this method estimates sediment ebullition rates using measured diffusive fluxes and assumed exponential profiles for CH_4 production in the sediment, as well as measured bubble composition to conduct a sediment mass balance for the upper portion of the sediment. In 2016 and 2017, ebullitive fluxes from sediments located 8 m below the surface were estimated using inverted funnels placed 4 m below the surface (Vachon et al. 2019). To estimate the total ebullition rate (R_{eb}) for 2016 and 2017, including the missing data from sediments above 8 m, we calculated the average proportion of total ebullition occurring below 8 m ($R_{\mathrm{eb}}/R_{\mathrm{eb,8m}} = \Phi_{8\mathrm{m}}$) using data from 2018 and 2019 as follows:

$$R_{\mathrm{eb}}(t) = F_{\mathrm{eb,8m}}(t) A_{\mathrm{s,8m}} \Phi_{8\mathrm{m}}; \quad \left[\mathrm{mmol\,d^{-1}}\right] \tag{7}$$

where $A_{\mathrm{s,8m}}$ and $F_{\mathrm{eb,8m}}$ are the sediment area and the ebullition flux below 8 m respectively. t are the dates of each sampling campaign conducted during 2016 and 2017.

The temporal variation of R_{eb} for 2018 and 2019 was estimated assuming that R_{eb} for July 2018 and August 2019 are the maximum rates during the respective years. The temporal distribution of the missing data of those years were obtained from the temporal distribution of 2016 as:

$$R_{\mathrm{eb,i}}(t) = R_{\mathrm{eb,i}}^{\max} \frac{R_{\mathrm{eb,2016}}(t)}{R_{\mathrm{eb,2016}}^{\max}}; \quad \left[\mathrm{mmol\,d^{-1}}\right] \tag{8}$$

where i is the year 2018 or 2019 and t is each sampling campaign conducted each year.

The bubble dissolution rates ($R_{\mathrm{dis}} \forall_{\mathrm{SML}}$) in the SML were estimated using the slope of the linear interpolation of the proportion of $R_{\mathrm{dis}} \forall_{\mathrm{SML}}$ in the SML and R_{eb} in May and August 2018 and July 2019 (Supporting Information Fig. S7). The R_{dis} rates for May and August 2018 and July 2019 were estimated following Ordóñez et al. (2023), where the dissolution from a single bubble released from the sediment was calculated using McGinnis et al. (2006) considering a 5-mm bubble diameter, which is an average bubble diameter observed in lakes.

Vertical CH_4 diffusive fluxes from/to the SML

Diffusive fluxes to/from the SML (F_z) were estimated using Fick's First Law:

$$F_z = -K_z \frac{\partial C}{\partial z}; \quad \left[\mathrm{mmol\,m^{-2}\,d^{-1}}\right] \tag{9}$$

where $\frac{\partial C}{\partial z}$ at the bottom of the SML was estimated using the water column profiles of CH_4 concentrations (Supporting Information Fig. S8). K_z was determined from the heat budget method (Powell and Jassby 1974) at the bottom of the SML using the CTD profiles and temperature measurements from the thermistor mooring located at M1.

Isotopic CH_4 mass balance

The isotopic signature associated to P_{net} ($\delta^{13}\mathrm{C}_{\mathrm{CH_4\text{-}P\_net}}$) was estimated using an isotopic CH_4 mass balance in the SML:

$$\begin{aligned} R_{\mathrm{bulk}} \delta^{13}\mathrm{C}_{\mathrm{CH_4-R_{bulk}}} = {} & \forall_{\mathrm{SML}} \left(R_{\mathrm{dis}} \delta^{13}\mathrm{C}_{\mathrm{CH_4-R_{dis}}} + P_{\mathrm{net}} \delta^{13}\mathrm{C}_{\mathrm{CH_4-P_{net}}}\right) \\ & + F_s A_s \delta^{13}\mathrm{C}_{\mathrm{CH_4-F_s}} + F_z A_p \delta^{13}\mathrm{C}_{\mathrm{CH_4-F_z}}; \left[\mathrm{mmol\,‰\,d^{-1}}\right] \end{aligned} \tag{10}$$

where $\delta^{13}\mathrm{C}_{\mathrm{CH_4-R_{bulk}}}$ is the result of the potential sources of CH_4 in the SML that include CH_4 diffused from the littoral sediment, released as bubbles and dissolved in the SML or vertically transported from the hypolimnion. Similarly, R_{bulk} is the rate of total production of CH_4 in the SML considering the different sources of CH_4 as:

$$R_{\mathrm{bulk}} = F_s A_s + F_z A_p + \forall_{\mathrm{SML}} (R_{\mathrm{dis}} + P_{\mathrm{net}}); \quad \left[\mathrm{mmol\,d^{-1}}\right] \tag{11}$$

where $\delta^{13}\mathrm{C}_{\mathrm{CH_4-F_s}}$, $\delta^{13}\mathrm{C}_{\mathrm{CH_4-F_z}}$ and $\delta^{13}\mathrm{C}_{\mathrm{CH_4-R_{dis}}}$ are the isotopic signatures at the top of the littoral sediment, at the bottom of the SML, and from bubbles dissolved in the SML, respectively. $\delta^{13}\mathrm{C}_{\mathrm{CH_4-F_z}}$ and $\delta^{13}\mathrm{C}_{\mathrm{CH_4-R_{dis}}}$ were extracted from Langenegger et al. (2022), whereas $\delta^{13}\mathrm{C}_{\mathrm{CH_4-F_z}}$ are extracted from water column profiles (Supporting Information Fig. S8) and $\delta^{13}\mathrm{C}_{\mathrm{CH_4-R_{bulk}}}$ from a Keeling plot using transect data measured in 2018 and 2019.

Oxidation rates and fraction of methane oxidized

Methane oxidation rates were estimated from Thottathil et al. (2019) as follows:

$$\ln(\mathrm{MOx}) = \beta_0 + \beta_1 \ln(\mathrm{CH_4}) + \beta_2 \frac{1}{T} + \ln\left(e^{-\lambda \mathrm{O_2}} - e^{-(\alpha+\lambda)\mathrm{O_2}}\right) \tag{12}$$

where MOx rates are in $\mathrm{mmol\,m^{-3}\,d^{-1}}$, CH_4, and oxygen (O_2) concentrations are in $\mathrm{mmol\,m^{-3}}$, and water temperature is in Kelvin. β_0, β_1, β_2, λ, and α were obtained from Thottathil et al. (2019).

The fraction of CH_4 oxidized (f_{ox}) was estimated from the Rayleigh model for closed systems (Liptay et al. 1998) using a constant fractionation factor ($\alpha = 1.02$; Bastviken et al. (2002) and Thottathil et al. 2018) and a constant isotopic signature of the mixture of sources determined via a Keeling plot ($\delta^{13}\mathrm{C}_{\mathrm{CH_4-Bulk}} = -59‰$). The closed system model is based on an isotopic mass balance assuming the SML as a closed single layer (i.e., volume of water) at some arbitrary time point of a large incubation experiment, and its applicability in surface water has been demonstrated (Thottathil et al. (2018)). We, however, also estimated f_{ox} using a mass balance approach ($f_{\mathrm{ox}} = \mathrm{MOx/Total\,Production}$) that uses measured sources (Table 1) during the campaigns along with oxidation rates estimated based on Thottathil et al. (2019).

Monte Carlo simulation

Monte Carlo simulations were performed (10,000 iterations) when solving both mass balance models following Ordóñez et al. (2023). P_{net}, R_{dis}, and F_z were selected within a normal distribution resulting from the mean (μ) and standard deviation (σ) retrieved from field measurements. To avoid negative values for F_a and F_s, a gamma distribution defined by the shape ($\kappa = \mu^2/\sigma^2$) and the scale ($\theta^2 = \sigma^2/\mu$) was chosen. Here the gamma distribution has the density $f(x) = \left(x^{\kappa-1}\frac{e^{-x/\theta}}{\theta^{\kappa}\Gamma}\right)$, where Γ is the gamma function. Random.normal and random.gamma functions from the Numpy package (Harris et al. 2020) in Python were used for each normal and gamma distributions, respectively.

Source contribution of atmospheric diffusive CH_4 fluxes

Each source contribution to the diffusive surface flux was estimated as:

$$\text{Source contribution}_i = \frac{S_i}{\sum_j S_j} \cdot 100; \quad [\%] \qquad (13)$$

where S_i is each source term (mol d^{-1}), such as bubble dissolution ($R_{\mathrm{dis}} \forall_{\mathrm{SML}}$), sediment flux ($F_s A_s$), net production/consumption ($P_{\mathrm{net}} \forall_{\mathrm{SML}}$), and vertical diffusive flux ($F_z A_z$). If $S_i \leq 0$, then $S_i = 0$ for each source term i.

Results

Limnological measurements

Surface waters remained oxygenated over the 4 yrs of measurements during the stratified period (2016–2019; Supporting Information Fig. S9). The surface water temperature during the stratified period was consistent between the different years with an average value of 21 ± 3 °C. The SML depth ranged between 1.4 and 7.5 m during the stratified period with a clear tendency to deepen towards the end of the summer (Supporting Information Fig. S10). The average Secchi disk depth (SD) and Chl *a* concentrations during the stratified period of the 4 yrs were 2.4 ± 1.1 m and 5.1 ± 3.1 mg m^{-3}, respectively (Supporting Information Table S1 and Fig. S11).

Surface CH_4 concentration and isotopic signature

The surface CH_4 concentrations ranged between 0.3 and 1.3 mmol m^{-3} during the stratified period with an average value of 0.93 ± 0.28 mmol m^{-3} (Supporting Information Fig. S12). In fact, the CH_4 concentrations showed a general tendency to be lower in May, increased in June and July, and decreased in September. There was a slight increase in CH_4 concentrations in October, likely due to the start of mixing (Fig. 2a). $\delta^{13}C_{CH_4}$ in the SML ranged between −60‰ and −30‰ with a tendency to become more enriched towards the end of the summer and beginning of autumn (Fig. 2b).

Higher surface CH_4 concentrations were observed in the transect conducted in July 2018 compared to May and September 2018, and August 2019 (Fig. 3). On average, the CH_4 concentrations near the shore were 7% higher than at the center of the lake, however the difference along each transect was not significant (ANOVA analysis). Surface $\delta^{13}C_{CH_4}$ along the transect ranged between −57‰ and −38‰ (Supporting Information Fig. S13). Lighter $\delta^{13}C_{CH_4}$ was observed in May 2018 compared with the other three campaigns (Supporting Information Fig. S13). Significant differences between $\delta^{13}C_{CH_4}$ at the shore and the center of the lake were only observed on August 2019, where $\delta^{13}C_{CH_4}$ near the shore was 8% more depleted than at the center (Supporting Information Fig. S13).

Diffusive CH_4 emissions to the atmosphere

Diffuse CH_4 emissions (F_{a}) at the air-water interface (AWI) measured with floating chambers ranged between 0.1 and 3.7 mmol m^{-2} d^{-1} during the stratified season (Table 3 and Supporting Information Fig. S14). On average, in September F_{a} reached its lowest value (1.0 ± 0.5 mmol m^{-2} d^{-1}) and increased during the fall up to 2.1 ± 14 mmol m^{-2} d^{-1} (Supporting Information Fig. S15a). The yearly average value of F_{a} during the stratified season was higher in 2016 (1.4 ± 1.0 mmol m^{-2} d^{-1}; number of days averaged $n = 5$) and 2017 (1.8 ± 0.8 mmol m^{-2} d^{-1}, $n = 6$) followed by a decrease during 2018 (1.0 ± 1.1 mmol m^{-2} d^{-1}, $n = 3$) and 2019 (0.5 ± 0.4 mmol m^{-2} d^{-1}, $n = 2$) (Supporting Information Fig. S15b). Using floating chamber measurements, we calculated the normalized chamber-based gas transfer coefficient ($k_{600,\mathrm{cb}}$) following (McGinnis et al. 2015) (Supporting Information Fig. S16), where the Schmidt number was estimated from surface water temperature (Wanninkhof 1992).

To estimate the diffusive CH_4 emissions for the wind-based model (Eq. 2), wind velocity at 10 m was used to calculate k_{CH_4} during 2016, 2017, and 2018 over the stratified period in Soppensee. Daily wind velocity at the Egolzwil meteorological station ranged between 0.6 and 7.8 m s^{-1} with an average value of 2 m s^{-1} (Supporting Information Fig. S17). The average value of k_{CH_4} estimated with MA10-NB was 1.3 ± 0.3 m s^{-1} from 2016 to 2018 with minimum and maximum values of 0.68 and 2.8 m s^{-1} respectively (Supporting Information Fig. S17). No significant differences were found between years for the wind velocity or k_{CH_4}. Five literature k_{600} parameterizations were compared with the chamber-based $k_{600,\mathrm{cb}}$ (Supporting Information Fig. S16) to determine the best k_{600} parameterization to be used in the wind-based mass balance model. The best fit between the k_{600} literature parameterizations and $k_{600,\mathrm{cb}}$ was obtained with MA10-NB (MacIntyre et al. (2010) negative buoyancy, $R^2 = 0.44$, MNB = 0.06). The other four parameterizations underestimate $k_{600,\mathrm{cb}}$ (MNB = [0.19–0.53]) and show a low determination coefficient ($R^2 = [-0.07$ to $0.44]$) (Supporting Information Table S2).

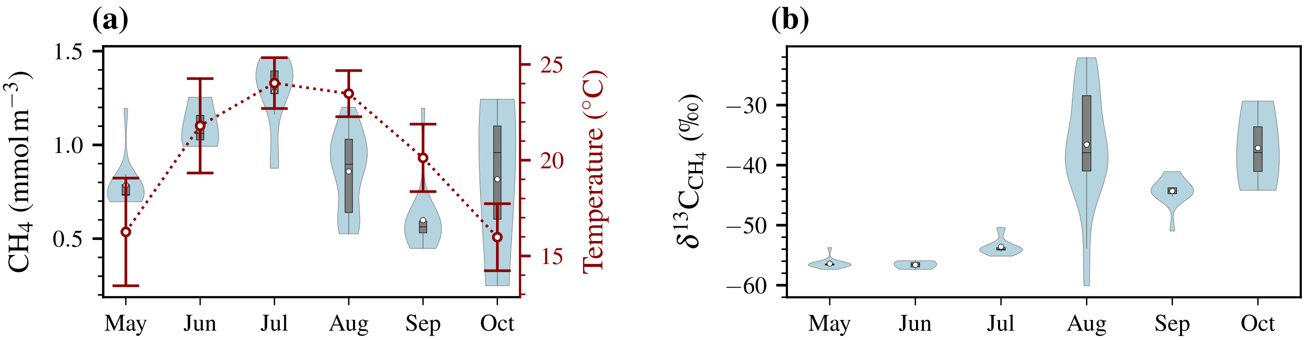

Fig. 2. (**a**) Monthly distribution of surface CH_4 concentrations (violin) and surface temperature (red line) from 2016 to 2019. (**b**) Monthly average of surface isotopic signature of CH_4 ($\delta^{13}C_{CH_4}$). Each box shows the first and third quartiles with the median (line), whiskers extend to the most extreme data point within 1.5 times the interquartile range from the box. The white dot represents the average of each distribution.

Diffusive CH_4 fluxes from littoral sediment

The deepest SML during the stratified season for all years was 7.5 m (October 2019); therefore, sediments in water shallower than 7.5 m were classified as littoral. Diffusive CH_4 fluxes from littoral sediments (F_s) were obtained via different methods (Table 2). The average F_s was $1.56 \pm 1.19\,\mathrm{mmol\,m^{-2}\,d^{-1}}$ for the entire 4-yr period. About 80% lower values were obtained with the Rhizons compared to the benthic chambers and cut-syringe methods. No correlation was observed between sampled depth and F_s within the SML depth range.

CH_4 ebullition rate and bubble dissolution

Monthly average ebullition rates ranged between 0.9 and $2.0\,\mathrm{mmol\,m^{-2}\,d^{-1}}$ (Supporting Information Fig. S18a) with the lowest in June and highest in September. Annually, the highest ebullitive fluxes were observed in 2018 ($2.3\,\mathrm{mmol\,m^{-2}\,d^{-1}}$) and the lowest in 2016 ($0.8\,\mathrm{mmol\,m^{-2}\,d^{-1}}$) (Supporting Information Fig. S18b). As the CH_4 dissolution rates were estimated based on the ebullitive fluxes and the McGinnis et al. (2006) bubble dissolution model, we observed the same temporal dynamics for dissolution rates as we did for ebullition. The dissolution rates into the SML layer ranged between 0.001 and $0.06\,\mu\mathrm{mol\,m^{-3}\,d^{-1}}$ (Table 3; Supporting Information Fig. S19).

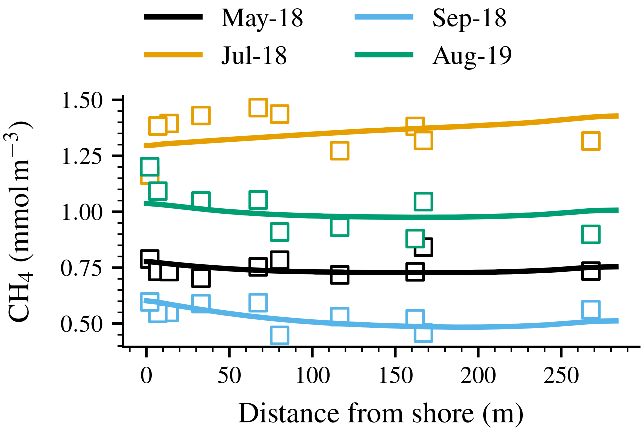

Fig. 3. Surface CH_4 concentration along the transect sampled in Soppensee. Lines represent the CH_4 concentration simulated using the lateral transport model and squares are the measured values.

Vertical diffusive fluxes from/to the SML

The vertical diffusive flux from/to the SML is driven by the vertical turbulent diffusivity K_z and the concentration gradient just below the bottom of the SML. K_z ranged between 0.1 and $8 \times 10^{-6}\,\mathrm{m^2\,s^{-1}}$ with a clear tendency to be lower towards the end of the summer (Supporting Information Figs. S20, S21). During the stratified season, F_z ranged between -0.11 and $0.22\,\mathrm{mmol\,m^{-2}\,d^{-1}}$ from 2016 to 2019 (Table 3; Supporting Information Fig. S22). Across all years, the metalimnion acted as a source of CH_4 to the SML in May, June and October and as a sink in August and September. In July of all years, F_z was negligible (Supporting Information Fig. S23a). During the stratified period in each sampling year, the metalimnion was a small source of CH_4 to the SML, except in 2017 (Supporting Information Fig. S23b).

Surface mass balance

The P_{net} rates obtained with the full-scale mass balance ($P_{net,fs}$), the wind-based ($P_{net,t}$) mass balance, and the lateral transport ($P_{net,lt}$) model ranged between -140 and $910\,\mu\mathrm{mol\,m^{-3}\,d^{-1}}$ (Fig. 4) and were similar across models (Supporting Information Fig. S24). Monte Carlo simulations were applied to assess uncertainties using all sources and sinks in the lateral transport model and the full-scale mass balance (Methods). A decrease in P_{net} rates was observed from the beginning towards the end of the summer where the highest and the lowest averaged P_{net} were estimated for June ($604 \pm 358\,\mu\mathrm{mol\,m^{-3}d^{-1}}$) and September ($-46 \pm 82\,\mu\mathrm{mol\,m^{-3}\,d^{-1}}$), respectively (Fig. 5). On average, P_{net}

Table 3. Inputs for the full-scale mass balance and lateral transport model in the surface mixed layer (SML) (mean ± SD).

Date	K_H	C_{hyp}	K_z	$\bar{k}_{CH_4}$	F_a	F_s	F_z	R_{dis}
	($m^2\ d^{-1}$)	($mmol\ m^{-3}$)	($10^{-6} m\ s^{-1}$)	($m\ d^{-1}$)	($mmol\ m^{-2}\ d^{-1}$)			($\mu mol\ m^{-3}\ d^{-1}$)
May 25, 2016					1.2 ± 0.4	1.6 ± 1.2 ($n = 6$)	0.1 ± 0.1	1.6 ± 10.8
June 15, 2016					1.4 ± 0.9		0.1 ± 0.1	7.5 ± 10.7
July 4, 2016					1.3 ± 1.2		0.0	11.1 ± 11.0
August 4, 2016					1.2 ± 0.8		−0.02 ± 0.01	28.1 ± 10.7
October 6, 2016					3.7 ± 0.4		0.02 ± 0.01	37.4 ± 11.0
May 22, 2017					2.9 ± 0.5		0.0	33.6 ± 10.9
June 12, 2017					1.4 ± 0.3		0.01 ± 0.01	45.6 ± 10.9
July 10, 2017					1.2 ± 0.3		−0.10 ± 0.04	23.2 ± 10.7
August 2, 2017					1.4 ± 0.6		−0.03 ± 0.02	27.8 ± 10.9
August 28, 2017					1.5 ± 1.0		−0.10 ± 0.03	51.1 ± 10.9
October 12, 2017					2.4 ± 0.8		0.2 ± 0.1	36.4 ± 10.7
May 16, 2018	5080	1.14	4.5	1.0	0.7 ± 0.2		0.10 ± 0.04	51.0 ± 3.9
July 10, 2018	5080	1.43	8.1	2.6	2.3 ± 1.4		0.1 ± 0.1	56.3 ± 10.8
September 12, 2018	5080	0.36	0.8	0.6	0.3 ± 0.2		0.0	58.3 ± 10.8
August 12, 2019	5080	0.18	2.6	1.1	0.6 ± 0.5		−0.1 ± 0.1	57.6 ± 8.4
October 22, 2019					0.2 ± 0.1		0.2 ± 0.1	54.9 ± 10.9

K_H is the horizontal dispersion coefficient, C_{hyp} is the CH_4 concentration 1 m below the SML, K_z is the vertical diffusivity at the base of the epilimnion, and $\bar{k}_{CH_4}$ is the average chamber-based mass transfer coefficient. F_a, F_s, F_z, and R_{dis} are the surface diffusive emissions, littoral sediment flux, vertical flux at the base of the epilimnion, and the bubble dissolution rate in the SML, respectively.

rates were about 350, 505, 174 and −7 $\mu mol\ m^{-3}\ d^{-1}$ for 2016, 2017, 2018, and 2019, respectively (Supporting Information Fig. S25). Note that only three campaigns were conducted in 2018 and two at the end of the stratified period of 2019. No simulation for the wind-based mass balance model was completed for 2019 given the lack of temporal data.

Isotopic CH_4 mass balance

The Keeling plot method (Keeling 1958) was applied to estimate the $\delta^{13}C_{CH_4}$ of the CH_4 mixture of sources in the SML ($\delta^{13}C_{CH_4-R_{bulk}}$) during the transects conducted in May, July and September 2018 and August 2019 (Fig. 6). When P_{net} rates were low (i.e., lower than 100 $\mu mol\ m^{-3} d^{-1}$, September 2018 and August 2019), the positive correlation between $1/CH_4$ and $\delta^{13}C_{CH_4}$ indicates CH_4 fractionation by MOx is occurring. In contrast, when P_{net} rates were high (May and July 2018), no positive correlation between $1/CH_4$ and $\delta^{13}C_{CH_4}$ was observed, thereby indicating that MOx was likely negligible compared to the CH_4 produced. Conducting an isotopic CH_4 mass balance in the SML, the $\delta^{13}C_{CH_4\text{-P\_net}}$ of the main source (P_{net} or OMP) was − 49‰ and − 53‰ for May and July 2018, respectively (the $\delta^{13}C_{CH_4}$ of all sources are summarized in Supporting Information Table S3).

Methane oxidation rates and fraction of methane oxidized

Estimated MOx rates from an empirical model developed by Thottathil et al. (2019) ranged between 0.01 and 0.2 $mmol\ m^{-3}\ d^{-1}$ (Fig. 7a). While no clear trend was observed in MOx rates, the fraction of CH_4 oxidized (f_{ox}) in the SML as calculated by both the Rayleigh model for closed systems and a mass balance approach tended to increase towards the end of summer into the fall (Fig. 7b).

Contribution of CH_4 sources to atmospheric diffusive emissions

Using the P_{net} obtained from the full-scale mass balance ($P_{net,fs}$), we calculated the contribution of each CH_4 source to atmospheric diffusive CH_4 emissions during the stratified season (Fig. 8). P_{net} and F_s were the major sources of CH_4 in the SML for most campaigns, with minor contributions from R_{dis} and F_z until the late summer campaigns of 2018 and 2019. On average, P_{net} contributed about 65% of the total diffusive emission from 2016 to 2019, ranging from negligible amounts in September 2018 and October 2019 up to 90% in May 2017. Seasonally, P_{net} contributions were generally higher at the beginning of summer (~ 80% in June) and decreased towards the end of summer. P_{net} was the dominant source at each campaign except September 2018 and August and October 2019, when the dominant source was F_s (September 2018 and October 2019) or R_{dis} (August 2019). On average, F_s contributed about 20% from 2016 to 2019 reaching up to about ~ 50% on September 2018. The seasonal F_s contribution mirrored the seasonal P_{net} contribution trend, that is, lower at the beginning of summer compared to the end. The contribution of bubble dissolution in the SML (R_{dis}) to diffusive CH_4

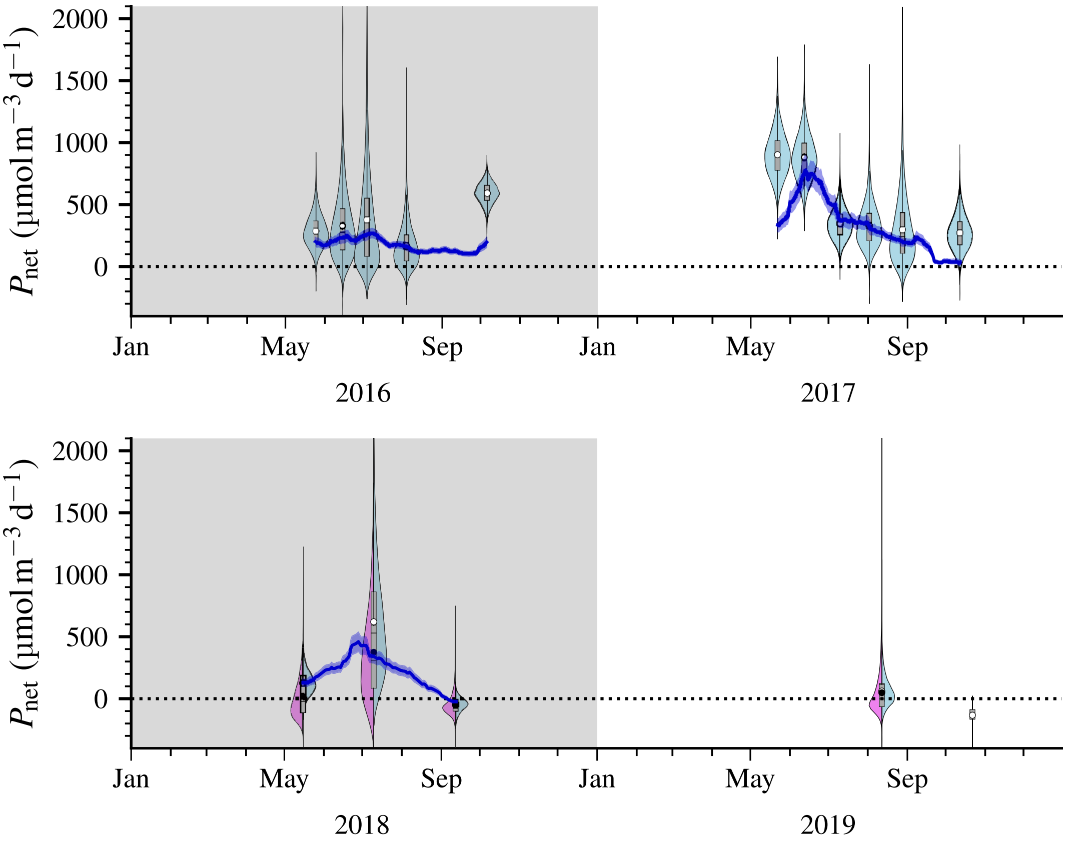

Fig. 4. P_{net} estimation during the stratified season using the full-scale mass balance ($P_{net,fs}$, light blue), the lateral transport model ($P_{net,lt}$, violet) and the wind-based mass balance model (two weeks moving average $P_{net,t}$, blue line). The shading around the wind-based mass balance model corresponds to an uncertainty based on using $0.55U_{10,Egolzwil}$ at the lower end and $0.85U_{10,Egolzwil}$ at the higher end for $U_{10,lake}$ when estimating surface diffusive emissions. Each box shows the first and third quartiles with the median (line), whiskers extend to the most extreme data point within 1.5 times the interquartile range from the box. The white and black dot represents the average of the distribution for the full-scale mass balance and lateral transport model, respectively. The P_{net} distributions are estimated from the Monte Carlo simulations.

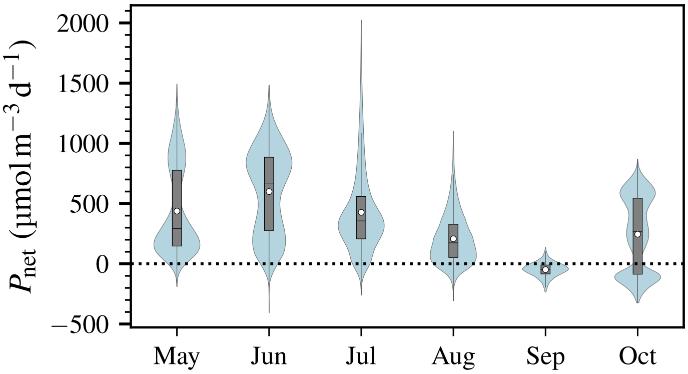

Fig. 5. Monthly average P_{net} rates in the SML during the stratified season from 2016 to 2019 obtained with the full-scale mass balance model. Each box shows the first and third quartiles with the median (line), whiskers extend to the most extreme data point within 1.5 times the interquartile range from the box. The P_{net} distributions are estimated from the Monte Carlo simulations. The white dot represents the average of the distribution. For better visualization the violin plots were filtered to show the data between two times the interquartile range. The non-filtered data are shown in Supporting Information Fig. S26.

emissions was negligible (< 0.1%) in 2016 and 2018, but was ~30% in 2018 and 2019. The highest R_{dis} contribution was on September 2018 (47%). The F_z contribution was negligible during the entire period of analysis, except for June 2018 and October 2019 when it was 10% and 30%, respectively.

Discussion

In this study, we calculated the rate of net CH_4 production/consumption (P_{net}) over 4 yrs in the oxic SML of a eutrophic Swiss lake using a full-scale mass balance, a wind-based mass balance, and a 1-D lateral transport model. The different approaches produced similar P_{net} rates and the same temporal patterns (Fig. 4). Except for the two 2019 campaigns, P_{net} rates were consistently positive during the strongly stratified period, indicating that OMP needs to occur to close the mass balance in Soppensee's SML. The average P_{net} rates for the four stratified seasons was 290 ± 358 µmol m^{-3} d^{-1} which is within the range of previously reported values ($0.2 - 1434$ µmol m^{-3} d^{-1};

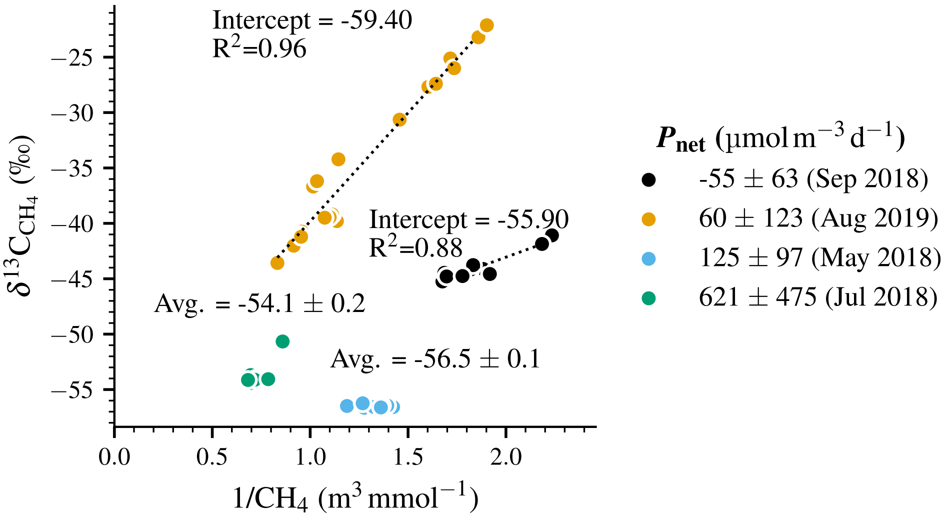

Fig. 6. Keeling plot analysis of the surface CH_4 concentration during the transects conducted in May, July, and September 2018 and August 2019. The different colors represent the P_{net} rates obtained on those dates with the full-scale mass balance model.

Günthel et al. (2021) and Ordóñez et al. (2023)). In fact, a highly similar P_{net} rate was estimated for another eutrophic Swiss lake (Lake Bretaye, 305 µmol m^{-3} d^{-1}; Ordóñez et al. (2023)). Moreover, P_{net} was the major contributor to diffusive atmospheric CH_4 emissions from Soppensee (65% ± 29%). As also shown by Vachon et al. (2019), the contribution of CH_4 produced in deep sediments to the SML is negligible during stratification (Fig. 8; Supporting Information Fig. S10) because deep CH_4 accumulates in the hypolimnion and/or is oxidized at the oxycline, and is therefore not transported to the SML (Vachon et al. 2019).

Monthly CH_4 dynamics in the SML over the stratified season

P_{net} rates in Soppensee during the stratified period were temporally variable. The wind-based and the full-scale mass balance models resulted in high P_{net} rates (~800 µmol m^{-3} d^{-1}) at the beginning of summer, indicating that OMP dominated over

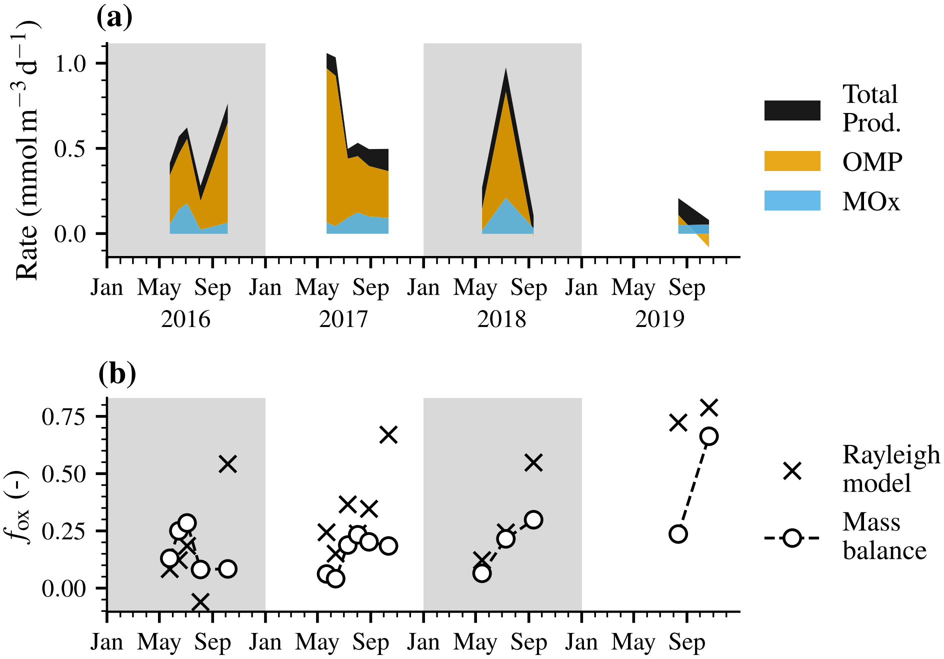

Fig. 7. Methane oxidation (MOx) dynamics during the stratified period from 2016 to 2019. (**a**) Rates of total production ($\mathrm{TotalProd.} = (F_s A_s + F_z A_z)/\forall_{SML} + P_{net} + \mathrm{MOx} + R_{dis}$), OMP and MOx in black, yellow and light blue, respectively. (**b**) Fraction of methane oxidized calculated from the Rayleigh model for closed systems (x; Liptay et al. (1998)) and our mass balance approach (circle; $f_{ox} = \mathrm{MOx}/\mathrm{TotalProd.}$).

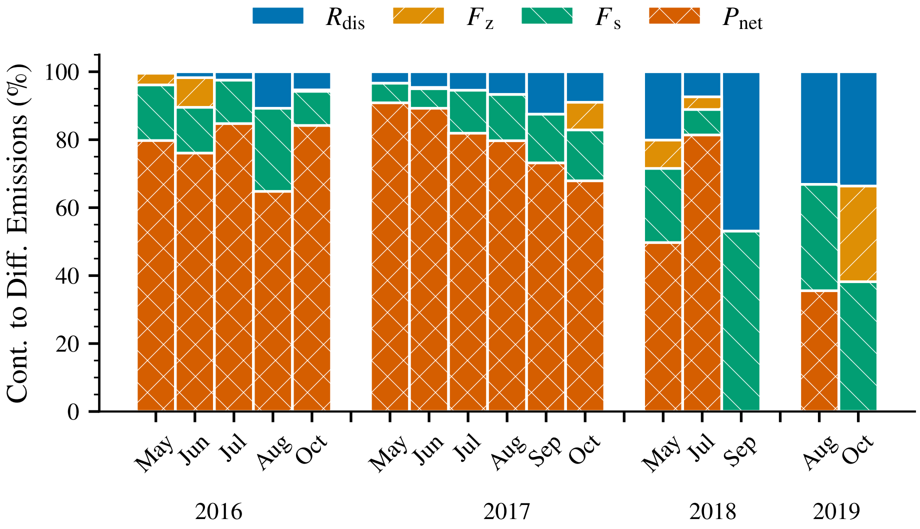

Fig. 8. Contribution to diffusive atmospheric CH_4 emissions (F_a) from the sediment flux (F_s), diffusive flux from hypolimnion (F_z), bubble dissolution (R_{dis}) and net production/consumption (P_{net}) in the SML using values from the full-scale mass balance.

MOx in Soppensee surface waters (Figs. 1a, 5). However, almost negligible rates were observed towards the end of the stratified season (Figs. 1b, 5), indicating that either the OMP rates decreased, the MOx increased or both. The same temporal trend was also observed by Liu et al. (2024), Ordóñez et al. (2023) and Günthel et al. (2019). The $\delta^{13}C_{CH_4}$ signature suggests that MOx likely dominated at the end of the stratified season as the residual CH_4 pool became highly ^{13}C-enriched, which is a typical sign of MOx (Reeburgh 2007). Although the mechanisms behind OMP and its impact on the $\delta^{13}C_{CH_4}$ signature of CH_4 pools are not clear, our mass balance results suggest that MOx can dominate over OMP in the SML of Soppensee during the latter part of the stratified period (Figs. 2b, 4).

Effect of P_{net} on $\delta^{13}C_{CH_4}$ values in the SML

Enriched $\delta^{13}C_{CH_4}$ in the SML at the end of the stratified season results from the $\delta^{13}C_{CH_4}$ of the different sources, MOx rates and its contribution to the CH_4 budget (Fig. 2b). Except for October 2016, total CH_4 production rates tended to decrease at the end of the summer, while no clear tendency was found for MOx rates (Fig. 7a). Therefore, the decrease of total production, which is dominated by OMP, and not an increase of MOx rates (Fig. 7a) would explain the increase of f_{ox} towards the end of the stratified season (Fig. 7b). While these methods do not allow us to accurately determine OMP and MOx rates given our assumptions, from a qualitative perspective these results suggest that OMP decreases when the SML is exposed to lower average light conditions due to the deeper SML, less daytime hours, and lower average solar angle at the end of the stratified season. While a strong positive relationship between OMP and light intensities and duration have been shown in marine phytoplankton (Klintzsch et al. 2020), to our knowledge, no studies have been conducted on freshwater phytoplankton.

Untangling MOx from P_{net} rates to estimate OMP rates in lake systems is challenging. Glass bottle incubations have been used to estimate MOx and OMP rates (Bižić et al. 2020; Günthel et al. 2020), but it is still unclear how representative the results of these methods are for lake environments. An alternative approach to estimate OMP and MOx rates is to conduct an isotopic mass balance, using the isotopic signatures of each CH_4 source in the SML and its measured fluxes. Unfortunately, high uncertainties remain regarding the $\delta^{13}C_{CH_4}$ values associated with OMP in freshwater systems (Thottathil et al. 2022; Klintzsch et al. 2023). Here we found negligible MOx rates in May and July 2018 based on the Keeling plot (Fig. 6), but we were able to estimate that the $\delta^{13}C_{CH_4}$ values associated with P_{net} or OMP ranged between – 49‰ and – 53‰. While these results are consistent with recent findings (Thottathil et al. 2022; Klintzsch et al. 2023), other studies have suggested less enriched values for $\delta^{13}C_{CH_4}$ associated to OMP (Bogard et al. 2014; Repeta et al. 2016). Therefore, process-based experiments are needed to better estimate $\delta^{13}C_{CH_4}$ and OMP and MOx rates at an ecosystem level.

Oxic methane contribution to diffusive emissions

OMP has been reported in several aquatic ecosystems, including the ocean (Karl et al. 2008; Li et al. 2020), rivers (Alowaifeer et al. 2023), high altitude (Perez-Coronel and Beman 2020) and pre-alpine lakes (Ordóñez et al. 2023), as well as lakes in temperate and arctic regions (DelSontro et al. 2018; Li et al. 2019). In addition, OMP has been observed using different methodologies, such as mesocosms (Bogard et al. 2014; Günthel et al. 2019), in-situ water incubations (Grossart et al. 2011; Bižić et al. 2020; Günthel et al. 2020), mass balances (Donis et al. 2017;

Günthel et al. 2019) and lateral transport models (Ordóñez et al. 2023). Despite growing evidence, the OMP contribution to diffusive CH_4 emissions from inland waters remains debated (Günthel et al. 2021; Peeters and Hofmann 2021). In our study, P_{net} was the greatest contributor to diffusive CH_4 fluxes to the atmosphere (F_a), reaching up to ~ 90% in May 2017 with an average value of ~ 65%. The temporal dynamics of the P_{net} contribution to diffusive emissions does not always follow the same trends as P_{net} rates. For example, in 2016, the P_{net} contribution to diffusive emissions was consistently around ~ 80%, while in 2017 the P_{net} contribution decreased throughout the stratified season (Fig. 8). Unfortunately, we do not have enough data in 2018 and 2019 to investigate the temporal dynamics of P_{net} contribution.

OMP key drivers and upscaling approach evaluation

Ordóñez et al. (2023) proposed an upscaling approach relating Chl *a*, light climate (LC) and Secchi depth (SD) to the ratio of P_{net} and surface CH_4 concentration. We tested this relationship using the monthly average data from Soppensee (Supporting Information Fig. S27) and observed a positive but lower correlation coefficient ($R^2 = 0.56$) than Ordóñez et al. (2023). Nevertheless, this positive relationship between Chl *a* concentrations, light conditions, and P_{net}/C_{CH_4} suggests that photosynthesis plays a role in OMP, which is in agreement with the recent finding that photoautotrophs can produce CH_4 (Bižić et al. 2020; Günthel et al. 2020; Hartmann et al. 2020; Klintzsch et al. 2020). Moreover, when we include the data from Soppensee on Fig. 6 from Ordóñez et al. (2023), a good correlation was observed ($R^2 = 0.83$, Supporting Information Fig. S28), implying that this approach could be potentially useful as a first estimate of P_{net} rates at a global scale. As the current OMP dataset is still sparse, future studies should be included to verify this trend on a larger scale.

Model comparison

The major advantage of the full-scale mass balance is that it only depends on measured values for its boundary conditions but assumes that these measurements are representative during the residence time of CH_4 in the SML (~ 14 d). While the full-scale mass balance does not consider horizontal dispersion, the good agreement with the lateral transport model ($P_{net,lt}$; Fig. 4; Supporting Information Fig. S24) suggests that advection or alterations in lateral transport parameterizations would primarily affect the distribution of mass within the lake and have minimal impact on P_{net} calculations. Moreover, consistent agreement between modeled and measured concentrations along transects supports the model's reliability.

In general, we observed a good agreement between the full-scale and the wind-based mass balance, except for May and Oct 2016 and 2017 when $P_{net,t}$ was lower than $P_{net,fs}$ (Fig. 4). This discrepancy is likely because k_{CH_4} estimated via the literature parameterization was lower than that estimated via chamber on those days (Supporting Information Fig. S17). The chamber-based k_{CH_4} thus better reflects the local temporal conditions rather than the temporal average value provided by the literature parameterization (e.g., Oct 2016 data). However, this discrepancy also points out a limitation of the k_{600} literature parameterizations that neglects different phenomena, such as diffusive flux enhancement (McGinnis et al. 2015) by oxygen microbubbles (Melack and Kilham 1974; Koschorreck et al. 2017) or buoyancy effects due to heating at low wind speeds (MacIntyre et al. 2021). A good agreement was found between the full-scale mass balance $P_{net,fs}$ and the lateral transport model $P_{net,lt}$. This latter approach accounts for the spatial variability of surface CH_4 concentrations and horizontal transport from littoral sediments using a constant k_{CH_4}. Therefore, considering these spatial changes does not have a great impact on P_{net} estimations.

Uncertainty assessment

P_{net} rates were estimated using three methodologies: a full-scale mass balance, a wind-based mass balance, and a lateral transport model. P_{net} distribution for each measuring time was estimated using Monte Carlo simulations, which integrated all the uncertainties from sources and sinks of CH_4 into P_{net} estimations. Although we observed high uncertainty in the P_{net} rate, except for May, September 2018 and August and October 2019, all the quartiles of P_{net} distribution were positive. Therefore, the probability that an error in our measured sources and sinks could cause a false positive P_{net} rate is low.

Alternative hypotheses for the missing CH_4 source

The contribution of hydrological inputs to the surface budget of CH_4 was not considered in our analysis. Soppensee experiences an annual outflow of approximately $0.03\,m^3\,s^{-1}$ through a small stream, with no specific inflow (Gruber et al. 2000). Groundwater likely contributes to the entire lake CH_4 budget; however, these water masses are generally characterized as colder and saltier compared to surface water. Therefore, we hypothesize that groundwater enters at the hypolimnion and should not be a substantial source of CH_4 to the SML.

Density currents are advective processes that can transport CH_4 produced in the sediment or accumulated in the littoral zone and usually occur sporadically in autumn during the initial surface cooling (Doda et al. 2024). This process was already taken into account in the full-scale mass balance as our approach assumes that all the CH_4 produced in the littoral sediment is transported to the center of the lake and that the SML is well mixed laterally. Moreover, the good agreement between P_{net} estimated from the lateral transport model and the full-scale mass balance suggests that horizontal dispersion is a reliable method for estimating lateral transport. For this reason, density currents do not need to be explicitly included in our analysis.

The other major input that can affect P_{net} estimations is F_s. In this study, we used a constant value for F_s for all 4 yrs that was the average from using three different methods on core data from six locations in the SML over 2016, 2017 and 2019 (Table 2; Supporting Information Fig. S3). Our resulting value (1.56 ± 1.19 mmol m^{-2} d^{-1}) was well within the range of those reported in the literature (0.001–8.8 mmol m^{-2} d^{-1}, Huttunen et al. 2006; Bastviken et al. 2008; Peeters et al. 2019; Ordóñez et al. 2023). Using six different locations to estimate F_s in the SML provided a good representation of the average littoral sediment in Soppensee. In addition, three methods were used to estimate the average flux, minimizing the bias related with each method. For example, bubbles can be included when taking the sediment sample in the cut-syringe method or the influence of surrounding sediments in the Rizhons methods (Seeberg-Elverfeldt et al. 2005). F_s can also vary by the increase of CH_4 production in the sediment with increasing temperature (Nozhevnikova et al. 1997). However, our core measurements were conducted mostly in July and August when the highest water temperatures were measured, and thus the highest CH_4 production rate in littoral sediment would be expected. While this means that our F_s values were in the upper range of what is expected, this translates into our P_{net} estimates being conservative, as F_s is another source of CH_4 to the SML (Eqs. 1 and 3).

As F_s has been shown to be influential on P_{net} estimations and a source of debate regarding OMP (Donis et al. 2017; Peeters et al. 2019; Günthel et al. 2021; Peeters and Hofmann 2021), we used the full-scale mass balance ($P_{net,fs}$) to investigate the impact of F_s on our P_{net} estimations in Soppensee. If we assume that OMP is negligible (i.e. $P_{net} = 0$), we would need up to 20 times higher sediment fluxes to account for the measured diffusive CH_4 flux to the atmosphere (Fig. 9). This means that F_s would have to approach $F_s = \sim 30$ mmol m^{-2} d^{-1}, which exceeds the highest value reported for littoral sediment CH_4 fluxes by a factor of 3–4 (Peeters et al. 2019). We therefore conclude that the diffusive CH_4 flux from littoral sediment alone cannot account for the diffusive CH_4 flux to the atmosphere and that OMP needs to be included in the CH_4 budget of Soppensee.

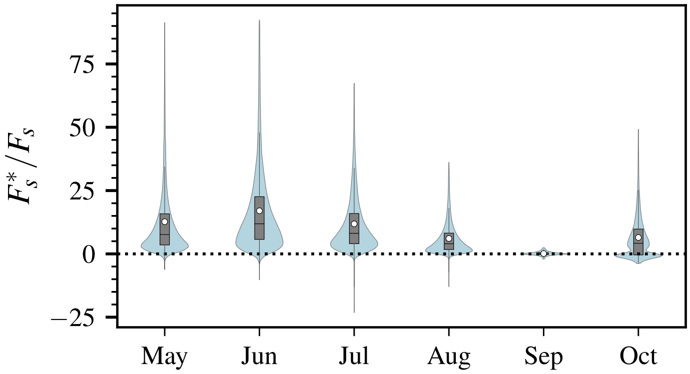

Fig. 9. Monthly average of the proportion of littoral sediment needed (F_s^*) to compensate the surface diffusive emissions compared to measured littoral sediment flux (F_s) considering no P_{net} in the surface mixed layer. The boxes show the first and third quartiles with the median (line), whiskers extend to most extreme data points within 1.5 times the interquartile range from the box. The white dot represents the average of the distributions. For better visualization the violin plots were filtered to show the data between two times the interquartile range. The non-filtered data are shown in Supporting Information Fig. S29.

Conclusions

Substantial evidence has been gathered over the past decade suggesting that OMP is a process that occurs in a variety of aquatic environments. However, P_{net} rates have only been reported in a few lakes and in a short timescale. This study is the first to demonstrate that P_{net} (i.e., the balance between OMP and MOx) consistently dominants as a contributor to diffusive CH_4 emissions over multiple years, and supports the dominance of OMP observed in other systems during a single season or year (Donis et al. 2017; Günthel et al. 2019; Thottathil et al. 2022; Ordóñez et al. 2023). Our dataset also highlights the tendency of P_{net} rates to start high in the spring and decrease to nearly negligible rates by the end of the stratified season, possibly due to the decrease of OMP rather than MOx. This dynamic appears to be more common in eutrophic systems than in oligotrophic ones (Ordóñez et al. 2023). Therefore, to understand the variability of diffusive CH_4 emissions from lakes, it is imperative that we are able to resolve OMP dynamics and its interaction with biochemical processes occurring within the lake.

Finally, our study also reveals that photoautotrophs and light conditions may significantly influence CH_4 production in oxygenated waters and that the upscaling method proposed originally by Ordóñez et al. (2023) could be used as a first estimation of P_{net} for different lake environments. This estimation is thus useful as a first step in determining the potential for P_{net} in any system to contribute to surface CH_4 emissions, which is important seeing as freshwater systems are responsible for about ~20–40% of natural CH_4 emissions (Rosentreter et al. 2021; Saunois et al. 2024). As OMP is a CH_4 source near the air-water interface and associated with photoautotrophs, better understanding of the mechanisms, rates, and drivers of OMP from various aquatic systems is required to accurately predict future aquatic CH_4 emissions in the face of global climate change and other confounding anthropogenic issues such as eutrophication.

Author Contributions

César Ordóñez, Tonya DelSontro, and Daniel F. McGinnis initiated and designed the study, organized campaigns, performed sampling, and analyzed the data with significant contributions from Timon Langenegger, Alexandrine Massot, and Daphne Donis. César Ordóñez wrote the manuscript with editorial help and conceptual contributions from Alexandrine Massot, Tonya DelSontro, and Daniel F. McGinnis.

Acknowledgments

We would like to thank Aurora Pinto, Kam Tang, Roxane Fillion, Dominic Vachon, Daphne Donis, and Sabine Flury for their help during the fieldwork and laboratory measurements. Thanks to Ena Suarez for editorial input in the manuscript. The authors also thank Mr. Bernhard Pfyffer for his support of this study on Soppensee, giving us access to the lake and infrastructure. Funding for this study was provided by Swiss National Science Foundation (SNSF) Grants No. 200021_169899 (Methane Paradox) and 200021_160018 (Bubble Flux) and European Union's Horizon 2020 research and innovation program under the Marie Skłodowska-Curie grant agreement No. 788612 (TRIAGE). Open access funding provided by Université de Genève.

Conflicts of Interest

None declared.

References

Alowaifeer, A. M., Q. Wang, B. Bothner, R. J. Sibert, S. B. Joye, and T. R. McDermott. 2023. "Aerobic Methane Synthesis and Dynamics in a River Water Environment." *Limnology and Oceanography* 68: 1762–1774. https://doi.org/10.1002/lno.12383.

Bastviken, D., J. J. Cole, M. L. Pace, and M. C. Van der Bogert. 2008. "Fates of Methane from Different Lake Habitats: Connecting Whole-Lake Budgets and CH_4 Emissions." *Journal of Geophysical Research* 113: G02024. https://doi.org/10.1029/2007JG000608.

Bastviken, D., J. Ejlertsson, and L. Tranvik. 2002. "Measurement of Methane Oxidation in Lakes: A Comparison of Methods." *Environmental Science & Technology* 36: 3354–3361. https://doi.org/10.1021/es010311p.

Bernhardt, J., and G. Kirillin. 2013. "Seasonal Pattern of Rotation-Affected Internal Seiches in a Small Temperate Lake." *Limnology and Oceanography* 58: 1344–1360. https://doi.org/10.4319/lo.2013.58.4.1344.

Bižić, M., T. Klintzsch, D. Ionescu, et al. 2020. "Aquatic and Terrestrial Cyanobacteria Produce Methane." *Science Advances* 6: eaax5343. https://doi.org/10.1126/sciadv.aax5343.

Bogard, M. J., P. A. del Giorgio, L. Boutet, et al. 2014. "Oxic Water Column Methanogenesis as a Major Component of Aquatic CH_4 Fluxes." *Nature Communications* 5: 5350. https://doi.org/10.1038/ncomms6350.

Boudreau, B. P. 1997. Diagenetic Models and Their Implementation: Modelling Transport and Reactions in Aquatic Sediments. Berlin: Springer.

Broecker, W. S., and T.-H. Peng. 1974. "Gas Exchange Rates between Air and Sea." *Tellus* 26: 21–35. https://doi.org/10.3402/tellusa.v26i1-2.9733.

Conrad, R. 2009. "The Global Methane Cycle: Recent Advances in Understanding the Microbial Processes Involved." *Environmental Microbiology Reports* 1: 285–292. https://doi.org/10.1111/j.1758-2229.2009.00038.x.

Crusius, J., and R. Wanninkhof. 2003. "Gas Transfer Velocities Measured at Low Wind Speed over a Lake." *Limnology and Oceanography* 48: 1010–1017. https://doi.org/10.4319/lo.2003.48.3.1010.

DelSontro, T., P. A. del Giorgio, and Y. T. Prairie. 2018. "No Longer a Paradox: The Interaction between Physical Transport and Biological Processes Explains the Spatial Distribution of Surface Water Methane within and across Lakes." *Ecosystems* 21: 1073–1087. https://doi.org/10.1007/s10021-017-0205-1.

Diaz, B. P., B. Knowles, C. T. Johns, et al. 2021. "Seasonal Mixed Layer Depth Shapes Phytoplankton Physiology, Viral Production, and Accumulation in the North Atlantic." *Nature Communications* 12: 6634. https://doi.org/10.1038/s41467-021-26836-1.

Doda, T., C. L. Ramón, H. N. Ulloa, et al. 2024. "Lake Surface Cooling Drives Littoral-Pelagic Exchange of Dissolved Gases." *Science Advances* 10: eadi0617. https://doi.org/10.1126/sciadv.adi0617.

Donis, D., S. Flury, A. Stöckli, J. E. Spangenberg, D. Vachon, and D. F. McGinnis. 2017. "Full-Scale Evaluation of Methane Production under Oxic Conditions in a Mesotrophic Lake." *Nature Communications* 8: 1661. https://doi.org/10.1038/s41467-017-01648-4.

Encinas Fernández, J., F. Peeters, and H. Hofmann. 2016. "On the Methane Paradox: Transport from Shallow Water Zones Rather than In Situ Methanogenesis Is the Major Source of CH_4 in the Open Surface Water of Lakes." *Journal of Geophysical Research: Biogeosciences* 121: 2717–2726. https://doi.org/10.1002/2016JG003586.

Ernst, L., B. Steinfeld, U. Barayeu, et al. 2022. "Methane Formation Driven by Reactive Oxygen Species across all Living Organisms." *Nature* 603, no. 7901: 1–6. https://doi.org/10.1038/s41586-022-04511-9.

Fee, E. J., R. E. Hecky, S. E. M. Kasian, and D. R. Cruikshank. 1996. "Effects of Lake Size, Water Clarity, and Climatic Variability on Mixing Depths in Canadian Shield Lakes." *Limnology and Oceanography* 41: 912–920. https://doi.org/10.4319/lo.1996.41.5.0912.

Forster, P., T. Storelvmo, K. Armour, et al. 2021. "The Earth's Energy Budget, Climate Feedbacks, and Climate Sensitivity." In Climate Change 2021: The Physical Science Basis. Contribution of Working Group I to the Sixth Assessment Report of the Intergovernmental Panel on Climate Change, edited by V. Masson-Delmotte and B. Zhou, 923–1054. Cambridge: Cambridge University Press, pp. 923–1054, https://doi.org/10.1017/9781009157896.009.

Grossart, H.-P., K. Frindte, C. Dziallas, W. Eckert, and K. W. Tang. 2011. "Microbial Methane Production in Oxygenated Water Column of an Oligotrophic Lake." *PNAS* 108: 19657–19661. https://doi.org/10.1073/pnas.1110716108.

Gruber, N., B. Wehrli, and A. Wüest. 2000. "The Role of Biogeochemical Cycling for the Formation and Preservation of Varved Sediments in Soppensee (Switzerland)." *Journal of Paleolimnology* 24: 277–291. https://doi.org/10.1023/A:1008195604287.

Günthel, M., D. Donis, G. Kirillin, et al. 2019. "Contribution of Oxic Methane Production to Surface Methane Emission in Lakes and Its Global Importance." *Nature Communications* 10: 5497. https://doi.org/10.1038/s41467-019-13320-0.

Günthel, M., D. Donis, G. Kirillin, et al. 2021. "Reply to 'Oxic Methanogenesis Is Only a Minor Source of Lake-Wide Diffusive CH_4 Emissions from Lakes'." *Nature Communications* 12, no. 1: 1205. https://doi.org/10.1038/s41467-021-21216-1.

Günthel, M., I. Klawonn, J. Woodhouse, et al. 2020. "Photosynthesis-Driven Methane Production in Oxic Lake Water as an Important Contributor to Methane Emission." *Limnology and Oceanography* 65: 2853–2865. https://doi.org/10.1002/lno.11557.

Harris, C. R., K. J. Millman, S. J. van der Walt, et al. 2020. "Array Programming with NumPy." *Nature* 585: 357–362. https://doi.org/10.1038/s41586-020-2649-2.

Hartmann, J. F., M. Günthel, T. Klintzsch, et al. 2020. "High Spatiotemporal Dynamics of Methane Production and Emission in Oxic Surface Water." *Environmental Science & Technology* 54: 1451–1463. https://doi.org/10.1021/acs.est.9b03182.

Huttunen, J. T., T. S. Väisänen, S. K. Hellsten, and P. J. Martikainen. 2006. "Methane Fluxes at the Sediment–Water Interface in some Boreal Lakes and Reservoirs." *Boreal Environment Research* 11: 27–34.

Imberger, J. 1985. "The Diurnal Mixed Layer." *Limnology and Oceanography* 30: 737–770. https://doi.org/10.4319/lo.1985.30.4.0737.

Imboden, D. M., and A. Wüest. 1995. "Mixing Mechanisms in Lakes." In Physics and Chemistry of Lakes, edited by A. Lerman, D. M. Imboden, and J. R. Gat, 83–138. Berlin Heidelberg: Springer. https://doi.org/10.1007/978-3-642-85132-2_4.

Karl, D. M., L. Beversdorf, K. M. Björkman, M. J. Church, A. Martinez, and E. F. Delong. 2008. "Aerobic Production of Methane in the Sea." *Nature Geoscience* 1: 473–478. https://doi.org/10.1038/ngeo234.

Keeling, C. D. 1958. "The Concentration and Isotopic Abundances of Atmospheric Carbon Dioxide in Rural Areas." *Geochimica et Cosmochimica Acta* 13: 322–334. https://doi.org/10.1016/0016-7037(58)90033-4.

Khatun, S., T. Iwata, H. Kojima, et al. 2019. "Aerobic Methane Production by Planktonic Microbes in Lakes." *Science of the Total Environment* 696: 133916. https://doi.org/10.1016/j.scitotenv.2019.133916.

Klintzsch, T., H. Geisinger, A. Wieland, et al. 2023. "Stable Carbon Isotope Signature of Methane Released from Phytoplankton." *Geophysical Research Letters* 50: e2023GL103317.

Klintzsch, T., G. Langer, A. Wieland, et al. 2020. "Effects of Temperature and Light on Methane Production of Widespread Marine Phytoplankton." *Journal of Geophysical Research: Biogeosciences* 125, no. 9: e2020JG005793. https://doi.org/10.1029/2020JG005793.

Koschorreck, M., I. Hentschel, and B. Boehrer. 2017. "Oxygen Ebullition from Lakes." *Geophysical Research Letters* 44: 1–7. https://doi.org/10.1002/2017GL074591.

Lamontagne, R. A., J. W. Swinnerton, V. J. Linnenbom, and W. D. Smith. 1973. "Methane Concentrations in Various Marine Environments." *Journal of Geophysical Research* 78: 5317–5324. https://doi.org/10.1029/JC078i024p05317.

Langenegger, T., D. Vachon, D. Donis, and D. F. McGinnis. 2019. "What the Bubble Knows: Lake Methane Dynamics Revealed by Sediment Gas Bubble Composition." *Limnology and Oceanography* 64: 1526–1544. https://doi.org/10.1002/lno.11133.

Langenegger, T., D. Vachon, D. Donis, and D. F. McGinnis. 2022. "Methane Oxidation Dynamics in a Stratified Lake: Insights Revealed from a Mass Balance and Carbon Stable Isotopes." *Limnology and Oceanography* 67: 2157–2173. https://doi.org/10.1002/lno.12195.

Li, W., J. E. Dore, A. J. Steigmeyer, et al. 2019. "Methane Production in the Oxygenated Water Column of a Perennially Ice-Covered Antarctic Lake." *Limnology and Oceanography* 65: 143–156. https://doi.org/10.1002/lno.11257.

Li, Y., C. G. Fichot, L. Geng, M. G. Scarratt, and H. Xie. 2020. "The Contribution of Methane Photoproduction to the Oceanic Methane Paradox." *Geophysical Research Letters* 47: e2020GL088362. https://doi.org/10.1029/2020GL088362.

Liptay, K., J. Chanton, P. Czepiel, and B. Mosher. 1998. "Use of Stable Isotopes to Determine Methane Oxidation in Landfill Cover Soils." *Journal of Geophysical Research, [Atmospheres]* 103: 8243–8250. https://doi.org/10.1029/97JD02630.

Liu, L., X. Zhang, S. Schorn, et al. 2024. "Strong Subseasonal Variability of Oxic Methane Production Challenges Methane Budgeting in Freshwater Lakes." *Environmental Science & Technology* 58: 19690–19701. https://doi.org/10.1021/acs.est.4c07413.

Lorke, A., P. Bodmer, C. Noss, et al. 2015. "Technical Note: Drifting Versus Anchored Flux Chambers for Measuring Greenhouse Gas Emissions from Running Waters." *Biogeosciences* 12: 7013–7024. https://doi.org/10.5194/bg-12-7013-2015.

Lotter, A. F. 1989. "Evidence of Annual Layering in Holocene Sediments of Soppensee, Switzerland." *Aquatic Sciences* 51: 19–30. https://doi.org/10.1007/BF00877778.

MacIntyre, S., J. H. F. Amaral, and J. M. Melack. 2021. "Enhanced Turbulence in the Upper Mixed Layer under Light Winds and Heating: Implications for Gas Fluxes." *Journal of Geophysical Research: Oceans* 126: e2020JC017026. https://doi.org/10.1029/2020JC017026.

MacIntyre, S., A. Jonsson, M. Jansson, J. Aberg, D. E. Turney, and S. D. Miller. 2010. "Buoyancy Flux, Turbulence, and the Gas Transfer Coefficient in a Stratified Lake."

Geophysical Research Letters 37: L24604. https://doi.org/10.1029/2010GL044164.

McGinnis, D. F., J. Greinert, Y. Artemov, S. E. Beaubien, and A. Wüest. 2006. "Fate of Rising Methane Bubbles in Stratified Waters: How Much Methane Reaches the Atmosphere?" *Journal of Geophysical Research: Oceans* 111: 1–15. https://doi.org/10.1029/2005JC003183.

McGinnis, D. F., G. Kirillin, K. W. Tang, et al. 2015. "Enhancing Surface Methane Fluxes from an Oligotrophic Lake: Exploring the Microbubble Hypothesis." *Environmental Science & Technology* 49: 873–880. https://doi.org/10.1021/es503385d.

Melack, J. M., and P. Kilham. 1974. "Photosynthetic Rates of Phytoplankton in East African Alkaline, Saline Lakes." *Limnology and Oceanography* 19: 743–755. https://doi.org/10.4319/lo.1974.19.5.0743.

Morana, C., S. Bouillon, V. Nolla-Ardèvol, et al. 2020. "Methane Paradox in Tropical Lakes? Sedimentary Fluxes Rather than Pelagic Production in Oxic Conditions Sustain Methanotrophy and Emissions to the Atmosphere." *Biogeosciences* 17: 5209–5221. https://doi.org/10.5194/bg-17-5209-2020.

Nozhevnikova, A. N., C. Holliger, A. Ammann, and A. J. B. Zehnder. 1997. "Methanogenesis in Sediments from Deep Lakes at Different Temperatures (2–70°C)." *Water Science and Technology* 36: 57–64. https://doi.org/10.1016/S0273-1223(97)00507-6.

Ordóñez, C. 2023. "Evaluation of the Methane Paradox in Four Adjacent Pre-Alpine Lakes across a Trophic Gradient." Version v1.0.0. Zenodo. https://doi.org/10.5281/zenodo.7695166.

Ordóñez, C., T. DelSontro, T. Langenegger, D. Donis, E. L. Suarez, and D. F. McGinnis. 2023. "Evaluation of the Methane Paradox in Four Adjacent Pre-Alpine Lakes across a Trophic Gradient." *Nature Communications* 14: 2165. https://doi.org/10.1038/s41467-023-37861-7.

Peeters, F., J. Encinas Fernandez, and H. Hofmann. 2019. "Sediment Fluxes Rather than Oxic Methanogenesis Explain Diffusive CH_4 Emissions from Lakes and Reservoirs." *Scientific Reports* 9: 243. https://doi.org/10.1038/s41598-018-36530-w.

Peeters, F., and H. Hofmann. 2015. "Length-Scale Dependence of Horizontal Dispersion in the Surface Water of Lakes." *Limnology and Oceanography* 60: 1917–1934. https://doi.org/10.1002/lno.10141.

Peeters, F., and H. Hofmann. 2021. "Oxic Methanogenesis Is Only a Minor Source of Lake-Wide Diffusive CH_4 Emissions from Lakes." *Nature Communications* 12: 1206. https://doi.org/10.1038/s41467-021-21215-2.

Perez-Coronel, E., and J. M. Beman. 2020. "Biogeochemical and Omic Evidence for Multiple Paradoxical Methane Production Mechanisms in Freshwater Lakes." bioRxiv. 2020.07.28.225276. https://doi.org/10.1101/2020.07.28.225276.

Powell, T., and A. Jassby. 1974. "The Estimation of Vertical Eddy Diffusivities below the Thermocline in Lakes." *Water Resources Research* 10: 191–198. https://doi.org/10.1029/WR010i002p00191.

Reeburgh, W. S. 2007. "Oceanic Methane Biogeochemistry." *Chemical Reviews* 107: 486–513. https://doi.org/10.1021/cr050362v.

Repeta, D. J., S. Ferrón, O. A. Sosa, et al. 2016. "Marine Methane Paradox Explained by Bacterial Degradation of Dissolved Organic Matter." *Nature Geoscience* 9: 884–887. https://doi.org/10.1038/ngeo2837.

Rosentreter, J. A., A. V. Borges, B. R. Deemer, et al. 2021. "Half of Global Methane Emissions Come from Highly Variable Aquatic Ecosystem Sources." *Nature Geoscience* 14: 225–230. https://doi.org/10.1038/s41561-021-00715-2.

Sander, R. 2015. "Compilation of Henry's Law Constants (Version 4.0) for Water as Solvent." *Atmospheric Chemistry and Physics* 15: 4399–4981. https://doi.org/10.5194/acp-15-4399-2015.

Saunois, M., A. Martinez, B. Poulter, et al. 2024. "Global Methane Budget 2000–2020." *Earth System Science Data Discussions*: 1–147. https://doi.org/10.5194/essd-2024-115.

Schubert, C. J., T. Diem, and W. Eugster. 2012. "Methane Emissions from a Small Wind Shielded Lake Determined by Eddy Covariance, Flux Chambers, Anchored Funnels, and Boundary Model Calculations: A Comparison." *Environmental Science & Technology* 46: 4515–4522. https://doi.org/10.1021/es203465x.

Scranton, M. I., and P. G. Brewer. 1977. "Occurrence of Methane in the Near-Surface Waters of the Western Subtropical North-Atlantic." *Deep Sea Research* 24: 127–138. https://doi.org/10.1016/0146-6291(77)90548-3.

Seeberg-Elverfeldt, J., M. Schlüter, T. Feseker, and M. Kölling. 2005. "Rhizon Sampling of Porewaters near the Sediment-Water Interface of Aquatic Systems: Rhizon Porewater Sampling." *Limnology and Oceanography: Methods* 3: 361–371. https://doi.org/10.4319/lom.2005.3.361.

Tang, K. W., D. F. McGinnis, K. Frindte, V. Brüchert, and H.-P. Grossart. 2014. "Paradox Reconsidered: Methane Oversaturation in Well-Oxygenated Lake Waters." *Limnology and Oceanography* 59: 275–284. https://doi.org/10.4319/lo.2014.59.1.0275.

Thottathil, S. D., P. C. J. Reis, P. A. del Giorgio, and Y. T. Prairie. 2018. "The Extent and Regulation of Summer Methane Oxidation in Northern Lakes." *Journal of Geophysical Research: Biogeosciences* 123: 3216–3230. https://doi.org/10.1029/2018JG004464.

Thottathil, S. D., P. C. J. Reis, and Y. T. Prairie. 2019. "Methane Oxidation Kinetics in Northern Freshwater Lakes." *Biogeochemistry* 143: 105–116. https://doi.org/10.1007/s10533-019-00552-x.

Thottathil, S. D., P. C. J. Reis, and Y. T. Prairie. 2022. "Magnitude and Drivers of Oxic Methane Production in Small Temperate Lakes." *Environmental Science & Technology* 56: 11041–11050. https://doi.org/10.1021/acs.est.2c01730.

Tilbrook, B. D., and D. M. Karl. 1995. "Methane Sources, Distributions and Sinks from California Coastal Waters to the Oligotrophic North Pacific Gyre." *Marine Chemistry* 49: 51–64. https://doi.org/10.1016/0304-4203(94)00058-L.

Vachon, D., T. Langenegger, D. Donis, and D. F. McGinnis. 2019. "Influence of Water Column Stratification and Mixing Patterns on the Fate of Methane Produced in Deep Sediments of a Small Eutrophic Lake." *Limnology and Oceanography* 64: 2114–2128. https://doi.org/10.1002/lno.11172.

Virtanen, P., R. Gommers, T. E. Oliphant, et al. 2020. "SciPy 1.0: Fundamental Algorithms for Scientific Computing in Python." *Nature Methods* 17: 261–272. https://doi.org/10.1038/s41592-019-0686-2.

Wang, Q., J. E. Dore, and T. R. McDermott. 2017. "Methylphosphonate Metabolism by *Pseudomonas* sp. Populations Contributes to the Methane Oversaturation Paradox in an Oxic Freshwater Lake." *Environmental Microbiology* 19: 2366–2378. https://doi.org/10.1111/1462-2920.13747.

Wanninkhof, R. 1992. "Relationship between Wind Speed and Gas Exchange over the Ocean." *Journal of Geophysical Research* 97: 7373–7382. https://doi.org/10.1029/92JC00188.

Wiesenburg, D. A., and N. L. Guinasso. 1979. "Equilibrium Solubilities of Methane, Carbon Monoxide, and Hydrogen in Water and Sea Water." *Journal of Chemical & Engineering Data* 24: 356–360. https://doi.org/10.1021/je60083a006.

Supporting Information

Additional Supporting Information may be found in the online version of this article.

Submitted 06 February 2024
Revised 02 September 2024
Accepted 16 February 2025